

Turing patterns in Matrix-Weighted Networks

Anna Gallo,^{1,2} Wilfried Segnou,³ and Timoteo Carletti^{3,*}

¹*IMT School for Advanced Studies, Piazza San Francesco 19, 55100 Lucca (Italy)*

²*INdAM-GNAMPA Istituto Nazionale di Alta Matematica ‘Francesco Severi’, P.le Aldo Moro 5, 00185 Rome (Italy)*

³*Department of mathematics and Namur Institute for Complex Systems, naXys*

University of Namur, Rue Grafé 2, B5000 Namur (Belgium)

(Dated: February 16, 2026)

Diffusion-driven instability is a fundamental mechanism underlying pattern formation in spatially extended systems. In almost all existing works, diffusion across the links of the underlying network is modeled through scalar weights, possibly complemented by cross-diffusion terms that are homogeneous across links. In this work, we investigate the emergence of Turing patterns on Matrix Weighted Networks (MWNs), a recently introduced framework in which each edge is associated with a matrix weight. Focusing on the class of coherent MWNs, we provide a novel characterization of coherence in terms of node-dependent orthonormal matrices, showing that link transformations can be written as relative rotations between nodes. This representation allows us to deal with coherent MWNs of any size and to introduce an orthonormal change of variables capable to reduce diffusion on a coherent MWN to diffusion on a standard weighted network with scalar weights. Building on this, we extend the classical Turing instability analysis to MWNs and derive the conditions under which a homogeneous equilibrium of the local dynamics loses stability due to matrix-weighted diffusion. Our results show how network topology, scalar weights, and inter-node transformations jointly shape pattern formation, and provide a constructive framework to analyze and design Turing patterns on matrix-weighted and higher-order networked systems.

I. INTRODUCTION

Beautiful and colorful patterns emerge spontaneously in Nature and in human-made devices; they are the result of the interaction among the many basic units constituting the system [1–3]. Very often, they originate from local reactions responsible for the creation and destruction of units, coupled with (long-range) diffusion capable of moving them apart. In this framework sits the elegant theory developed by Alan Turing in the context of morphogenesis [4] and later extended to study self-organization in more general systems: under suitable conditions, any tiny, spatially dependent perturbation applied to a stable homogeneous stationary equilibrium, will drive the latter to a new, possibly patchy, solution, i.e., the spatial Turing pattern [3]. The diffusion mechanism being the destabilizing factor, the above process is also known in the literature as a diffusion-driven instability.

The interaction among the basic units constituting the system, can thus be modeled by means of reaction-diffusion equations that govern the deterministic evolution of the concentrations both in time and space, the latter being a regular substrate [5] or a discrete one, e.g., a complex network [6].

Since the work by Nakao and Mikhailov [6], scholars have studied the conditions for the emergence of Turing patterns in diverse scenarios ranging from directed networks [7] to non-normal ones [8, 9], passing through multiplex networks [10–12]. Motivated by the increasing interest in higher-order networks [13–17], Turing patterns

have been studied on hypergraphs [18], simplicial complexes [19], higher-order structures [20, 21] and recently in the framework of topological signals [22, 23] (the interested reader can consult [24] for a recent review about Turing patterns on networks and higher-order networks).

In all the above mentioned works the “connections” of the underlying substrate, being links of a network of some higher-order counterpart, i.e., hyperedges or simplices, carry scalar weights that multiply species densities to encode the role of diffusion coefficients. A relevant and different case is the one where cross-diffusion is at play [25–28], namely, each node, or spatial location, receives a linear combination of species densities from each incoming link. In the case the state of each node is described by a d -dimensional vector, this process can be realized by multiplying the latter by a suitable $d \times d$ matrix. It is thus natural to consider that in the diffusion process, species densities undergo a transformation. To the best of our knowledge, in the literature, one can only find results dealing with the same “diffusion” matrix for all links in the framework of cross-diffusion models. In this work, we make one step further and consider the emergence of Turing patterns in the case where each link could be endowed with a different transformation matrix, by exploiting the recently introduced framework of *Matrix Weighted Networks* [29, 30] (MWN).

Our results apply to the class of MWNs satisfying the coherence condition [29]. Roughly speaking, the latter implies that any signal propagating through multiple oriented paths in a MWN always returns to its starting point without distortion, i.e., the product of the matrices weights across an oriented cycle is the identity. In this work, we will show that the dynamical system should preserve the MWN coherence, determining thus a strong in-

* timoteo.carletti@unamur.be

teraction between dynamics and structure [17]. To check the coherence condition can be computationally costly, for this reason we prove an alternative characterization of coherent WMNs allowing us to build WMNs of any sizes, filling in this way the existing gap limiting scholars to considered only small WMNs, where coherence can be checked by hand.

Turing instability manifests once the diffusive-like coupling is capable to turn unstable an otherwise locally stable spatially homogeneous solution. The coherence of a MWN and its invariance by the dynamics allow to show the existence of a suitable change of variables, thanks to which one can prove the existence of such stable spatially homogeneous solution. By resorting to a linear stability analysis about the latter solution, we can determine conditions on the spectrum of the MWN Laplace matrix to ensure the emergence of Turing patterns.

The work is organized as follows. In the next Section II we introduce the notion of coherent MWN and we prove an alternative characterization of the latter. Section III is devoted to the develop Turing theory in the framework of WMNs. Section IV is divided into three parts, each aimed at applying the theory presented so far to a chosen dynamical system, the Stuart-Landau model IV A, an abstract model with a given rotation invariance IV B, and the Lorenz model IV C. Finally, we summarize our findings and conclude in Section V.

II. CHARACTERIZATION OF WEIGHTED MATRIX NETWORKS

The aim of this section is to briefly introduce *Matrix Weighted Networks* (WMNs) [29], present a novel characterization of coherent WMNs, and introduce the main tools we need to develop a Turing theory for dynamical systems coupled via WMNs. As in [29], we restrict our attention to reciprocal interactions. Accordingly, without loss of generality, we present the discussion in terms of symmetric (undirected) networks.

Let $G = (V, E, \{\mathbf{W}_{ij}\}_{i,j=1}^n)$ be a MWN with $n = |V|$ nodes and $m = |E|$ edges. To any existing edge, $(i, j) \in E$, we associate a weighted matrix $\mathbf{W}_{ij} \in \mathbb{R}^{d \times d}$ defined as

$$\mathbf{W}_{ij} = w_{ij} \mathbf{R}_{ij}, \quad (1)$$

where $w_{ij} := \|\mathbf{W}_{ij}\|_2 > 0$ is the scalar weight and $\mathbf{R}_{ij} \in \mathbb{R}^{d \times d}$ is a transformation, such that $\|\mathbf{R}_{ij}\|_2 = 1$. In the following, we assume the latter to belong to the group of rotations and $\mathbf{W}_{ij} = \mathbf{W}_{ji}^\top$ for all i and j , meaning $w_{ij} = w_{ji}$ and $\mathbf{R}_{ij} = \mathbf{R}_{ji}^\top$.

Let $d_i = \sum_j w_{ij}$ denote the strength of node i , and define the *supra-degree matrix* $\mathcal{D} = \mathbf{D} \otimes \mathbf{I}_d$, where $\mathbf{D} = \text{diag}(d_1, \dots, d_n)$, \mathbf{I}_d is the d -dimensional identity matrix and \otimes denotes the Kronecker product. We can

then define the *supra-Laplace matrix* as

$$\mathcal{L} = \mathcal{D} - \mathcal{W}, \quad (2)$$

where \mathcal{W} is the *supra-weight matrix*, which has a block structure, with the (i, j) -block being \mathbf{W}_{ij} .

Coherence condition and characterization of coherent MWN. A MWN is said to be *coherent* [29] if, for every oriented cycle composed by k different edges, $\mathcal{C} := ((i_1, i_2), (i_2, i_3), \dots, (i_k, i_1))$, the product of the transformation matrices along the cycle equals the identity, i.e.,

$$\prod_{(i,j) \in \mathcal{C}} \mathbf{R}_{ij} = \mathbf{I}_d. \quad (3)$$

This property implies that nodes can be partitioned into distinct groups, with the transformation along any walk between nodes within the same group being the identity. Furthermore, the transformation from any node in one group to any node in another group is the same.

In a coherent MWN, one can define the block diagonal matrix \mathcal{S} , where the i -th block is the $d \times d$ matrix, \mathbf{O}_{1i} , representing the product of transformations, i.e., rotations in the present setting, along any oriented walk starting from node 1 and ending at node i (see Eq. (15) below for further details). Since the composition of rotations is itself a rotation, each \mathbf{O}_{1i} is also a rotation. Importantly, because of the coherence condition, the choice of the first node can be arbitrary (for the sake of convenience, we hereby label it as node 1), and if several paths exist, the choice of the walk is also arbitrary and does not affect the results. Moreover, in the partition associated with the MWN, the matrix \mathbf{O}_{1i} represents the composed transformation between any node in the group to which 1 belongs and any node in the group of i . To check that a given MWN is coherent can be, in principle, computationally costly because it requires to verify (3) for all paths; for this reason the theory has been so far applied only to simple hand-made examples of coherent MWN [29, 30]. One goal of this work is to fill this gap and to propose an algorithm capable to create coherent MWN of any size, based on the following proposition.

Proposition 1 (Characterization of coherent WMNs). *Let G be a MWN, whose topology is given by an oriented, symmetric network. The following are equivalent.*

(a) *There exist n orthonormal matrices $\mathbf{Q}_1, \dots, \mathbf{Q}_n \in \mathcal{O}(d)$ such that, for every edge $(i, j) \in E$,*

$$\mathbf{W}_{ij} = w_{ij} \mathbf{Q}_i^\top \mathbf{Q}_j, \quad (4)$$

namely $\mathbf{R}_{ij} = \mathbf{Q}_i^\top \mathbf{Q}_j$.

(b) *For every $(i, j) \in E$, the link matrix \mathbf{R}_{ij} is orthonormal and, for any oriented cycle $\mathcal{C} = ((v_0, v_1), (v_1, v_2), \dots, (v_{\ell-1}, v_\ell))$ in G , with $v_\ell = v_0$,*

$$\prod_{t=1}^{\ell} \mathbf{R}_{v_{t-1} v_t} = \mathbf{I}_d, \quad (5)$$

i.e., the graph G is coherent.

Proof. (a) \Rightarrow (b). Assume that there exist orthonormal matrices $\mathbf{Q}_1, \dots, \mathbf{Q}_n \in O(d)$ such that $\mathbf{W}_{ij} = w_{ij} \mathbf{Q}_i^\top \mathbf{Q}_j$ for all $(i, j) \in E$. Then, for any $(i, j) \in E$ we can define

$$\mathbf{R}_{ij} = \mathbf{Q}_i^\top \mathbf{Q}_j, \quad (6)$$

which is orthonormal, being the product of orthonormal matrices. Now, consider any path $P : i = v_0, v_1, \dots, v_\ell = j$. The product of transformations along the path is

$$\begin{aligned} \prod_{t=1}^{\ell} \mathbf{R}_{v_{t-1} v_t} &= \prod_{t=1}^{\ell} \mathbf{Q}_{v_{t-1}}^\top \mathbf{Q}_{v_t} \\ &= \mathbf{Q}_i^\top \left(\prod_{t=1}^{\ell-1} \mathbf{Q}_{v_t} \mathbf{Q}_{v_t}^\top \right) \mathbf{Q}_j = \mathbf{Q}_i^\top \mathbf{Q}_j. \end{aligned} \quad (7)$$

If $i = j$, the path is a cycle, and the product equals \mathbf{I}_d , confirming the coherence condition holds.

(b) \Rightarrow (a). Assume that for every edge $(i, j) \in E$, \mathbf{R}_{ij} is orthonormal, and, for every cycle \mathcal{C} , the product of the rotations along it is the identity \mathbf{I}_d . Fix a reference node $k \in V$ and select an arbitrary orthonormal matrix \mathbf{Q}_k (e.g., \mathbf{I}_d). For each $j \in V$, consider a path $P_{kj} : k = v_0, v_1, \dots, v_\ell = j$, and define

$$\tilde{\mathbf{Q}}_j := \mathbf{Q}_k \mathbf{R}_{P_{kj}}, \quad \mathbf{R}_{P_{kj}} := \prod_{s=1}^{\ell} \mathbf{R}_{v_{s-1} v_s}. \quad (8)$$

Notice that, if P'_{kj} is another path from k to j , concatenating P_{kj} and P'_{kj} forms a cycle. Then, by coherence,

$$\mathbf{R}_{P_{kj}} \mathbf{R}_{P'_{kj}}^{-1} = \mathbf{I}_d, \quad (9)$$

so $\mathbf{R}_{P_{kj}} = \mathbf{R}_{P'_{kj}}$ and $\tilde{\mathbf{Q}}_j$ is well defined.

By construction,

$$\tilde{\mathbf{Q}}_i^\top \tilde{\mathbf{Q}}_j = (\mathbf{Q}_k \mathbf{R}_{P_{ki}})^\top (\mathbf{Q}_k \mathbf{R}_{P_{kj}}) = \mathbf{R}_{P_{ki}}^\top \mathbf{R}_{P_{kj}}. \quad (10)$$

Now, for any edge $(i, j) \in E$, consider the cycle formed by concatenating the path P_{ki} , the edge (i, j) , and the reverse path P_{jk} . By coherence,

$$\mathbf{R}_{P_{ki}} \mathbf{R}_{ij} \mathbf{R}_{P_{jk}}^{-1} = \mathbf{I}_d. \quad (11)$$

Since $\mathbf{R}_{P_{jk}}$ is orthonormal, $\mathbf{R}_{P_{jk}}^{-1} = \mathbf{R}_{P_{jk}}^\top = \mathbf{R}_{P_{kj}}$. Therefore,

$$\mathbf{R}_{ij} = \mathbf{R}_{P_{ki}}^\top \mathbf{R}_{P_{kj}} = \tilde{\mathbf{Q}}_i^\top \tilde{\mathbf{Q}}_j. \quad (12)$$

□

Notice that the representation

$$\mathbf{R}_{ij} = \mathbf{Q}_i^\top \mathbf{Q}_j, \quad (i, j) \in E, \quad (13)$$

is unique up to a global orthonormal transformation. Indeed, if $\{\mathbf{Q}_i\}_{i=1}^n$ satisfy condition (a), then for any

$\mathbf{O} \in O(d)$ the matrices $\mathbf{Q}'_i = \mathbf{Q}_i \mathbf{O}$ define the same network, since

$$\mathbf{Q}'_i^\top \mathbf{Q}'_j = \mathbf{O}^\top \mathbf{Q}_i^\top \mathbf{Q}_j \mathbf{O} = \mathbf{Q}_i^\top \mathbf{Q}_j. \quad (14)$$

Thus, the family $\{\mathbf{Q}_i\}_{i=1}^n$ is determined only up to a right action of $O(d)$. For more details about the characterization of coherent MWNs, we refer the interested reader to Appendix A.

Supra-Laplace matrix and Identity-Transformed MWNs. Let us introduce the block diagonal matrix \mathcal{S} , whose i -th block is the $d \times d$ matrix, \mathbf{O}_{1i} , above defined in formula:

$$\mathcal{S} = \begin{pmatrix} \mathbf{I}_d & 0 & \dots & \dots & 0 \\ 0 & \mathbf{O}_{12} & \dots & \dots & 0 \\ \vdots & \vdots & \ddots & \vdots & \vdots \\ 0 & \dots & \dots & 0 & \mathbf{O}_{1n} \end{pmatrix}. \quad (15)$$

Let us observe that, in the following, without loss of generality, we will assume each block to contain a single node. On the contrary, if several nodes are contained in each block, the above formula is valid up to a small abuse of notation because we identified node i with the i -th block to which it belongs; this will not change the results, because all nodes in the i -th block are equivalent, being connected by links whose transformation is the identity matrix. This is the general MWNs framework introduced in [29].

Given any $\vec{u} \in \mathbb{R}^d$, the vector $\vec{U} = \mathcal{S}^\top (\vec{I}_n \otimes \vec{u})$ can be shown to be an eigenvector of the supra-Laplacian \mathcal{L} with eigenvalue 0 if and only if the MWN is coherent [29].

By using the matrix \mathcal{S} and the supra-Laplacian \mathcal{L} , we can define a second supra-Laplace matrix

$$\bar{\mathcal{L}} = \mathcal{S} \mathcal{L} \mathcal{S}^\top, \quad (16)$$

which corresponds to the supra-Laplace matrix where all the transformation matrices \mathbf{O} have been replaced by the identity matrix \mathbf{I}_d , as described in [29]. This new matrix depends only on the scalar weights and the topology of the network; indeed, it can be written as:

$$\bar{\mathcal{L}} = \bar{\mathbf{L}} \otimes \mathbf{I}_d, \quad (17)$$

where $\bar{\mathbf{L}} = \mathbf{D} - \mathbf{A}^{(w)}$, and $\mathbf{A}^{(w)}$ is the weighted adjacency matrix of the underlying network, i.e., each (i, j) -entry of $\mathbf{A}^{(w)}$ equals w_{ij} .

III. TURING THEORY ON MWNs

Let us consider a d -dimensional system whose state variable $\vec{x} \in \mathbb{R}^d$ evolves in time according to the ordinary differential equation (ODE)

$$\frac{d\vec{x}}{dt} = \vec{f}(\vec{x}), \quad (18)$$

where $\vec{f} : A \rightarrow \mathbb{R}^d$ is some nonlinear function and A an open subset of \mathbb{R}^d . Let us assume to have n identical copies of the above ODE, each one being identified by the state variable $\vec{x}_j \in \mathbb{R}^d$, $j = 1, \dots, n$, and assume moreover to couple them via a MWN. The time evolution of the state variable anchored to the i -th node, \vec{x}_i , is then described by

$$\begin{aligned} \frac{d\vec{x}_i}{dt} &= \vec{f}(\vec{x}_i) - \sum_j \mathcal{L}_{ij} \vec{h}(\vec{x}_j), \\ &= \vec{f}(\vec{x}_i) - \sum_j w_{ij} \mathbf{I}_d \vec{h}(\vec{x}_j) + \sum_j \mathbf{W}_{ij} \vec{h}(\vec{x}_j), \end{aligned} \quad (19)$$

where we hypothesized that the coupling function \vec{h} does not depend on the node index. By defining the vector $\vec{x} = (\vec{x}_1^\top, \dots, \vec{x}_n^\top)^\top \in \mathbb{R}^{nd}$, we can rewrite Eq. (19) as

$$\frac{d\vec{x}}{dt} = f_*(\vec{x}) - \mathcal{L}h_*(\vec{x}), \quad (20)$$

where f_* and h_* act component-wise resulting into a nd -dimensional vector, namely

$$f_*(\vec{x}) := (\vec{f}(\vec{x}_1)^\top, \dots, \vec{f}(\vec{x}_n)^\top)^\top, \quad (21)$$

and similarly for h_* .

A Turing instability occurs if system (20) admits a stable homogeneous stationary solution, $\vec{x}_j = \vec{x}^*$ for all $j = 1, \dots, n$, once we silence the coupling, i.e., we set $\mathcal{L} = 0$, that turns out unstable once the coupling is taken into account. The instability is therefore driven by the coupling and leads the system to a new equilibrium, possibly heterogeneous, i.e., spatially dependent, known as a Turing pattern.

Let us, thus, assume the ODE (18) possesses a stable stationary solution, \vec{x}^* , we would like the latter to be also a solution of the coupled system, namely $\vec{x}_j(t) \equiv \vec{x}^*$, for all $j = 1, \dots, n$ and $t \geq 0$, to solve (19). In the case the underlying support is a (connected) network with positive weight, then the above claim holds true [31–33] because the network Laplace matrix admits the eigenvector $\vec{1}_n = (1, \dots, 1)^\top \in \mathbb{R}^n$ with eigenvalue $\Lambda^{(1)} = 0$. For general MWNs the latter fact does not arise because the transformation matrices “mix” the components of the state vector; however one can “disentangle” those modes by showing that $\vec{X}^* = \mathcal{S}^\top(\vec{1}_n \otimes \vec{x}^*)$ is a stationary solution of (20). The latter claim holds true if the MWN is coherent [29, 30] and if the dynamical system (20) preserves the coherence, namely it is invariant with respect to the (product of) matrices \mathbf{R}_{ij} [30]. Namely, for all $i = 1, \dots, n$ and all $\vec{x} \in \mathbb{R}^d$, the following conditions must hold true:

$$\mathbf{O}_{1i} \vec{f}(\mathbf{O}_{1i}^\top \vec{x}) = \vec{f}(\vec{x}) \quad \text{and} \quad \mathbf{O}_{1i} \vec{h}(\mathbf{O}_{1i}^\top \vec{x}) = \vec{h}(\vec{x}). \quad (22)$$

The time derivative of \vec{X}^* clearly vanishes, being the

latter a constant vector. On the other hand, we have

$$\begin{aligned} \vec{f}_*(\vec{X}^*) - \mathcal{L}\vec{h}_*(\vec{X}^*) &= \begin{pmatrix} \vec{f}(\vec{x}^*) \\ \vec{f}(\mathbf{O}_{12}^\top \vec{x}^*) \\ \vdots \\ \vec{f}(\mathbf{O}_{1n}^\top \vec{x}^*) \end{pmatrix} - \mathcal{L} \begin{pmatrix} \vec{h}(\vec{x}^*) \\ \vec{h}(\mathbf{O}_{12}^\top \vec{x}^*) \\ \vdots \\ \vec{h}(\mathbf{O}_{1n}^\top \vec{x}^*) \end{pmatrix} \\ &= \begin{pmatrix} \vec{f}(\vec{x}^*) \\ \mathbf{O}_{12}^\top \vec{f}(\vec{x}^*) \\ \vdots \\ \mathbf{O}_{1n}^\top \vec{f}(\vec{x}^*) \end{pmatrix} - \mathcal{L} \begin{pmatrix} \vec{h}(\vec{x}^*) \\ \mathbf{O}_{12}^\top \vec{h}(\vec{x}^*) \\ \vdots \\ \mathbf{O}_{1n}^\top \vec{h}(\vec{x}^*) \end{pmatrix}, \end{aligned}$$

where we used the invariance of \vec{f} and \vec{h} given by (22). We can thus conclude that

$$\begin{aligned} \vec{f}_*(\vec{X}^*) - \mathcal{L}\vec{h}_*(\vec{X}^*) &= \\ &= \mathcal{S}^\top(\vec{1}_n \otimes \vec{f}(\vec{x}^*)) - \mathcal{L}\mathcal{S}^\top(\vec{1}_n \otimes \vec{h}(\vec{x}^*)) = 0, \end{aligned} \quad (23)$$

because $\vec{f}(\vec{x}^*) = 0$ and $\mathcal{L}\mathcal{S}^\top(\vec{1}_n \otimes \vec{h}(\vec{x}^*)) = 0$.

The emergence of Turing patterns relies on the proof of the instability of the stationary solution \vec{X}^* . To achieve this goal we rewrite the (dn) -dimensional state vector as $\vec{x} = \vec{X}^* + \delta\vec{x}$, where $\delta\vec{x}$ is “small” perturbation; if $\delta\vec{x}(t)$ will converge to 0, then the equilibrium \vec{X}^* is locally stable, and unstable otherwise. The time evolution of $\delta\vec{x}$ can be obtained by performing a linear stability analysis of (20) about the stationary solution \vec{X}^* :

$$\frac{d\delta\vec{x}}{dt} = \mathbf{J}_{f_*}(\vec{X}^*) \delta\vec{x} - \mathcal{L}\mathbf{J}_{h_*}(\vec{X}^*) \delta\vec{x}, \quad (24)$$

where $\mathbf{J}_{f_*}(\vec{X}^*)$ and $\mathbf{J}_{h_*}(\vec{X}^*)$ are respectively the Jacobian of f_* and h_* evaluated on the equilibrium \vec{X}^* . The latter equation can be written in “components” by defining $\delta\vec{x} = (\delta x_1^\top, \dots, \delta x_n^\top)^\top$ and obtain

$$\frac{d\delta\vec{x}_j}{dt} = \mathbf{J}_f(\mathbf{O}_{1j}^\top \vec{x}^*) \delta\vec{x}_j - \sum_\ell \mathcal{L}_{j\ell} \mathbf{J}_h(\mathbf{O}_{1\ell}^\top \vec{x}^*) \delta\vec{x}_\ell, \quad (25)$$

The invariance condition (22) returns the following relations satisfied by the Jacobian matrices

$$\mathbf{J}_f(\mathbf{O}_{1j}^\top \vec{x}^*) = \mathbf{O}_{1j}^\top \mathbf{J}_f(\vec{x}^*) \mathbf{O}_{1j} \quad (26)$$

and

$$\mathbf{J}_h(\mathbf{O}_{1j}^\top \vec{x}^*) = \mathbf{O}_{1j}^\top \mathbf{J}_h(\vec{x}^*) \mathbf{O}_{1j}. \quad (27)$$

Hence, we can conclude that

$$\frac{d\delta\vec{x}_j}{dt} = \mathbf{O}_{1j}^\top \mathbf{J}_f(\vec{x}^*) \mathbf{O}_{1j} \delta\vec{x}_j - \sum_\ell \mathcal{L}_{j\ell} \mathbf{O}_{1\ell}^\top \mathbf{J}_h(\vec{x}^*) \mathbf{O}_{1\ell} \delta\vec{x}_\ell, \quad (28)$$

or equivalently by defining $\delta\vec{w}_j = \mathbf{O}_{1j} \delta\vec{x}_j$

$$\begin{aligned} \frac{d\delta\vec{w}_j}{dt} &= \mathbf{J}_f(\vec{x}^*) \delta\vec{w}_j - \sum_\ell \mathbf{O}_{1j} \bar{L}_{j\ell} \mathbf{O}_{1\ell}^\top \mathbf{J}_h(\vec{x}^*) \delta\vec{w}_\ell \\ &= \mathbf{J}_f(\vec{x}^*) \delta\vec{w}_j - \sum_\ell \bar{L}_{j\ell} \mathbf{J}_h(\vec{x}^*) \delta\vec{w}_\ell. \end{aligned} \quad (29)$$

In the following, we will refer to $\delta\vec{w}_j$ as “rotated” variables because of the application of the rotation matrices \mathbf{O}_{1j} onto the original variables, $\delta\vec{x}_j$. Let us observe that by using the stack vectors $\delta\vec{x}$ and $\delta\vec{w}$, the above change of variables can be rewritten as $\delta\vec{w} = \mathcal{S}\delta\vec{x}$. Let us finally observe that to get (29), we made use of the definition of the supra-Laplace matrix $\bar{\mathcal{L}}$.

To prove the stability of $\delta\vec{w}_j$ and hence of $\delta\vec{x}_j$, we exploit the existence of an orthonormal basis for the Laplace matrix $\bar{\mathbf{L}}$, i.e., $\bar{\phi}_j^{(\alpha)}$, $\Lambda^{(\alpha)}$, $\alpha = 1, \dots, n$, to project $\delta\vec{w}_j$ onto the latter

$$\delta\vec{w}_j = \sum_{\alpha} \delta\hat{w}_{\alpha} \bar{\phi}_j^{(\alpha)}. \quad (30)$$

In this way, Eq. (29) returns

$$\sum_{\alpha} \frac{d\delta\hat{w}_{\alpha}}{dt} \bar{\phi}_j^{(\alpha)} = \mathbf{J}_f(\vec{s}) \sum_{\alpha} \delta\hat{w}_{\alpha} \bar{\phi}_j^{(\alpha)} - \sum_{\alpha} \Lambda^{(\alpha)} \mathbf{J}_h(\vec{s}) \delta\hat{w}_{\alpha} \bar{\phi}_j^{(\alpha)}. \quad (31)$$

By left multiplying by $\bar{\phi}_j^{(\alpha)}$ and by using the orthonormality of eigenvectors we eventually obtain

$$\begin{aligned} \frac{d\delta\hat{w}_{\alpha}}{dt} &= \left[\mathbf{J}_f(\vec{x}^*) - \Lambda^{(\alpha)} \mathbf{J}_h(\vec{x}^*) \right] \delta\hat{w}_{\alpha} \quad \forall \alpha = 1, \dots, n \\ &=: \mathbf{J}_{\alpha} \delta\hat{w}_{\alpha}. \end{aligned} \quad (32)$$

The above linear system contains the information about the dynamics and the coupling via the Jacobian matrices, while the MWN enters only via the eigenvalues of the supra-Laplace matrix $\bar{\mathcal{L}}$, depending only on the scalar weights. The perturbation $\delta\vec{w}_j$ does not converge to zero if there exists at least one α for which $\delta\hat{w}_{\alpha}$ does not converge to zero either.

In conclusion, by defining the *dispersion relation*, $\lambda(\Lambda^{(\alpha)})$, to be the largest real part of the eigenvalues of the matrix \mathbf{J}_{α} , then the existence of α such that

$\lambda(\Lambda^{(\alpha)}) > 0$ determines the instability conditions we were looking for.

In the remaining sections, we will present the above theory applied to three relevant dynamical systems, but its validity clearly goes beyond those examples.

IV. RESULTS

The aim of this section is to introduce three systems and examine the conditions under which Turing instability can emerge as predicted by the theory developed above.

A. The Stuart–Landau model

The first system we take into account is the Stuart–Landau (SL) model [34–37], a canonical example of nonlinear oscillators widely used to describe a broad class of phenomena and resulting to be a normal form for systems close to a supercritical Hopf-bifurcation. For the application we want to describe, we will, however, consider the SL dynamics in the subcritical case, where, i.e., the origin is a stable equilibrium. For a detailed analysis and the explicit computations presented in this section, we refer to Appendix B.

In Cartesian coordinates, a single SL oscillator j can be written as

$$\begin{aligned} \frac{d}{dt} \begin{pmatrix} x_j \\ y_j \end{pmatrix} &= \begin{pmatrix} \sigma_{\text{Re}} & -\sigma_{\text{Im}} \\ \sigma_{\text{Im}} & \sigma_{\text{Re}} \end{pmatrix} \begin{pmatrix} x_j \\ y_j \end{pmatrix} \\ &\quad - (x_j^2 + y_j^2) \begin{pmatrix} \beta_{\text{Re}} & -\beta_{\text{Im}} \\ \beta_{\text{Im}} & \beta_{\text{Re}} \end{pmatrix} \begin{pmatrix} x_j \\ y_j \end{pmatrix}, \end{aligned} \quad (33)$$

where we introduced the complex model parameters $\sigma = \sigma_{\text{Re}} + i\sigma_{\text{Im}}$ and $\beta = \beta_{\text{Re}} + i\beta_{\text{Im}}$.

Here, we consider n identical SL oscillators anchored to the nodes of a MWN, coupled via a diffusive-like nonlinear function. The dynamics of the j -th unit is thus given by

$$\begin{aligned} \frac{d}{dt} \begin{pmatrix} x_j \\ y_j \end{pmatrix} &= \begin{pmatrix} \sigma_{\text{Re}} & -\sigma_{\text{Im}} \\ \sigma_{\text{Im}} & \sigma_{\text{Re}} \end{pmatrix} \begin{pmatrix} x_j \\ y_j \end{pmatrix} - (x_j^2 + y_j^2) \begin{pmatrix} \beta_{\text{Re}} & -\beta_{\text{Im}} \\ \beta_{\text{Im}} & \beta_{\text{Re}} \end{pmatrix} \begin{pmatrix} x_j \\ y_j \end{pmatrix} - \sum_{\ell} \mathcal{L}_{j\ell} \left[(x_{\ell}^2 + y_{\ell}^2)^{\frac{m-1}{2}} \begin{pmatrix} \mu_{\text{Re}} & -\mu_{\text{Im}} \\ \mu_{\text{Im}} & \mu_{\text{Re}} \end{pmatrix} \begin{pmatrix} x_{\ell} \\ y_{\ell} \end{pmatrix} \right] \\ &=: \vec{f}(x_j, y_j) - \sum_{\ell} \mathcal{L}_{j\ell} \vec{h}(x_{\ell}, y_{\ell}), \end{aligned} \quad (34)$$

where $\vec{f}(x_j, y_j)$ is the nonlinear function defined by the above equation and $\vec{h}(x_{\ell}, y_{\ell}) := (x_{\ell}^2 + y_{\ell}^2)^{\frac{m-1}{2}} \begin{pmatrix} \mu_{\text{Re}} & -\mu_{\text{Im}} \\ \mu_{\text{Im}} & \mu_{\text{Re}} \end{pmatrix} \begin{pmatrix} x_{\ell} \\ y_{\ell} \end{pmatrix}$ defines the coupling function with complex coupling strength $\mu = \mu_{\text{Re}} + i\mu_{\text{Im}}$, and \mathcal{L}

is the supra-Laplace matrix of the MWN.

We define the underlying MWN by following the construction provided in Proposition 1 and focusing on the two-dimensional case ($d = 2$). More specifically, to each node i we associate an orthonormal matrix $\mathbf{R}_i \in \text{O}(2)$ and, for every pair of connected nodes (i, j) , we con-

struct the corresponding matrix-valued edge weights as $\mathbf{W}_{ij} = w_{ij} \mathbf{R}_{ij}$ where $w_{ij} \in \mathbb{R}$ is a scalar positive weight and the link transformation is defined by $\mathbf{R}_{ij} = \mathbf{R}_i^\top \mathbf{R}_j$. Note that \mathbf{R}_{ij} is orthonormal as the product of orthonormal matrices.

We can associate with the complex parameters σ , β and μ three real antisymmetric 2×2 matrices, and one can prove that they commute with any 2×2 orthonormal matrix \mathbf{R} . It thus follows

$$\vec{f}(\mathbf{R}\vec{x}) = \mathbf{R}\vec{f}(\vec{x}), \quad \vec{h}(\mathbf{R}\vec{x}) = \mathbf{R}\vec{h}(\vec{x}), \quad \forall \vec{x}, \quad (35)$$

and hence the dynamics preserve the coherent structure of the network.

The origin is clearly an equilibrium of (33) and one can prove that it is stable provided $\sigma_{\text{Re}} < 0$.

To determine the conditions for the onset of Turing instability, we linearize the coupled system (34) in the original coordinates (x_j, y_j) about the origin, then we perform the “rotation” to new coordinates (ξ_j, η_j) , i.e., $(\xi_1, \eta_1, \dots, \xi_n, \eta_n)^\top = \mathcal{S}(x_1, y_1, \dots, x_n, y_n)^\top$, and project the resulting system onto the Laplace eigenbasis

$$\xi_j = \sum_{\alpha} \hat{\xi}_{\alpha} \vec{\phi}_j^{(\alpha)}, \quad (36)$$

$$\eta_j = \sum_{\alpha} \hat{\eta}_{\alpha} \vec{\phi}_j^{(\alpha)}. \quad (37)$$

By exploiting the orthogonality of the eigenbasis, the resulting systems can be rewritten as

$$\begin{aligned} \frac{d}{dt} \begin{pmatrix} \hat{\xi}_{\alpha} \\ \hat{\eta}_{\alpha} \end{pmatrix} &= \left[\begin{pmatrix} \sigma_{\text{Re}} & -\sigma_{\text{Im}} \\ \sigma_{\text{Im}} & \sigma_{\text{Re}} \end{pmatrix} - \Lambda^{(\alpha)} \begin{pmatrix} \mu_{\text{Re}} & -\mu_{\text{Im}} \\ \mu_{\text{Im}} & \mu_{\text{Re}} \end{pmatrix} \right] \begin{pmatrix} \hat{\xi}_{\alpha} \\ \hat{\eta}_{\alpha} \end{pmatrix} \\ &=: \mathbf{M}(\Lambda^{(\alpha)}) \begin{pmatrix} \hat{\xi}_{\alpha} \\ \hat{\eta}_{\alpha} \end{pmatrix}. \end{aligned} \quad (38)$$

The diffusion-driven instability occurs when the real part of at least one eigenvalue of $\mathbf{M}(\Lambda^{(\alpha)})$ becomes positive for some $\alpha > 1$.

A direct computation allows to determine the eigenvalues of $\mathbf{M}(\Lambda^{(\alpha)})$, to be $\lambda_{\alpha} = (\sigma_{\text{Re}} - \Lambda^{(\alpha)} \mu_{\text{Re}}) \pm i(\sigma_{\text{Im}} - \Lambda^{(\alpha)} \mu_{\text{Im}})$ for any α . Since $\sigma_{\text{Re}} < 0$ and $\Lambda^{(\alpha)} \geq 0$, we thus have

$$\text{Re}(\lambda_{\alpha}) = \sigma_{\text{Re}} - \Lambda^{(\alpha)} \mu_{\text{Re}} > 0, \quad (39)$$

if μ_{Re} is sufficiently negative. Alternatively, once the model parameters σ_{Re} and μ_{Re} are fixed, the instability condition (39) holds true provided

$$\Lambda^{(\alpha)} > -\frac{\sigma_{\text{Re}}}{\mu_{\text{Re}}} =: \Lambda_{\text{crit}}, \quad (\text{with } \alpha > 1). \quad (40)$$

Notice that such a condition shows that modes associated to eigenvalues $\Lambda^{(\alpha)} > \Lambda_{\text{crit}}$ become unstable, leading to pattern formation, while the uniform mode ($\alpha = 1, \Lambda^{(1)} = 0$) remains stable since $\sigma_{\text{Re}} < 0$. Finally, by analyzing the radial dynamics of the SL oscillator, we can show that no stable limit cycle exists for $\sigma_{\text{Re}} < 0$. Hence, the observed instability cannot be attributed to

oscillatory behavior but is purely driven by the network coupling.

In Fig. 1 and Fig. 2, we provide numerical results supporting the analytical ones. In the former, the MWN is defined by using as underlying network obtained from a stochastic block model with $n = 50$ nodes divided into four groups. In the latter, the underlying topology of the MWN is generated by an Erdős–Rényi random graph. In both cases, top panels refer to the case where the dispersion relation is negative for all α , thus the perturbation shrinks to zero and the origin is stable, while bottom panels show the onset of diffusion-driven instabilities due to the presence of unstable eigenvalues, i.e., those that satisfy condition (40). Panels (a) and (b) of Fig. 1 and Fig. 2 clearly show a linear dispersion relation, note that the blue curve has been drawn only to help the reader to identify the linear trend. The instability threshold is crossed precisely when $\Lambda^{(\alpha)} = \Lambda_{\text{crit}} = -\sigma_{\text{Re}}/\mu_{\text{Re}}$, and this determines the emergence of patterns as clearly visible in panels (d) where we display the time evolution of $\xi_j(t)$, i.e., the real part of the complex signal $z_j(t)$ in the “rotated” variables.

B. Abstract model invariant under rotations by $2\pi/k$

Let us, now, consider an abstract model with a given rotational symmetry to be used to test the emergence of Turing patterns in MWNs. The model is inspired by the Stuart-Landau system, where the cubic nonlinearity has been replaced with a general $(k+1)$ -th power term, $k \geq 2$. More precisely, we consider

$$\frac{dz_j}{dt} = \sigma z_j + \beta z_j^{k+1} - \varepsilon \sum_{\ell} \mathcal{L}_{j\ell} z_{\ell}, \quad (41)$$

where $z_j \in \mathbb{C}$ describes the state of the j -th node, $j = 1, \dots, n$; σ , β and ε are complex parameters, $k \in \mathbb{N}$ determines the nonlinearity of the reaction part and \mathcal{L} is the supra-Laplace matrix of the MWN.

Once we silence the interaction via the MWN, we obtain for all $j = 1, \dots, n$ the system

$$\frac{dz_j}{dt} = \sigma z_j + \beta z_j^{k+1} \equiv f(z_j), \quad (42)$$

that admits the trivial equilibrium $z^{(0)} = 0$ and the k roots of the equation $z^k = -\sigma/\beta$

$$\hat{z}^{(s)} = \left(\frac{|\sigma|}{|\beta|} \right)^{\frac{1}{k}} e^{i \frac{\arg \sigma - \arg \beta}{k}} e^{i \pi \frac{1+2s}{k}} \quad \forall s = 1, \dots, k, \quad (43)$$

where we introduced $\sigma = |\sigma| e^{i \arg \sigma}$ and similarly for β . The stability of such equilibria can be determined by linearizing the system about the equilibrium, namely, to compute the derivative of $f(z)$ at the equilibrium we are interested in, and to impose its real part to be negative:

$$f'(z^{(s)}) = \sigma + (k+1)\beta(z^{(s)})^k = -\sigma k, \quad (44)$$

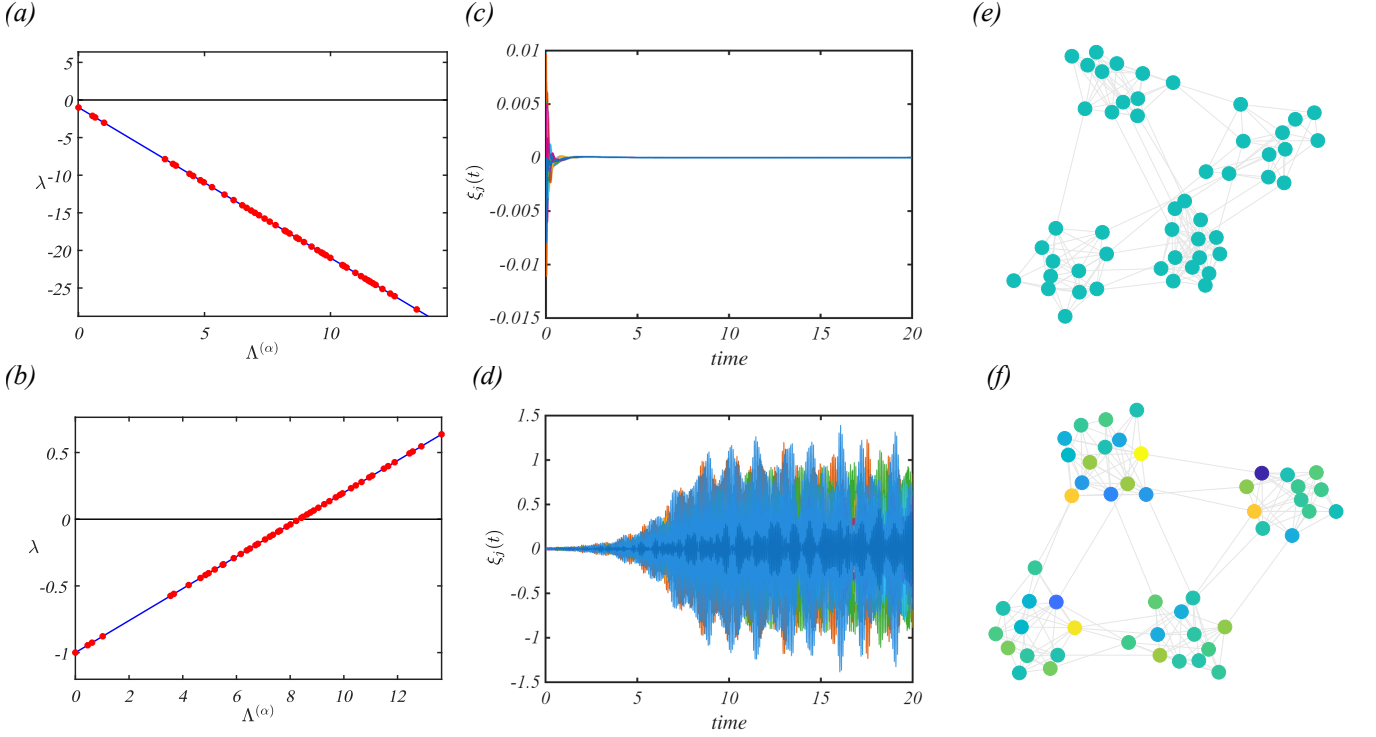


FIG. 1: **Emergence of Turing patterns in a MWN with stochastic block model topology of coupled Stuart-Landau systems.** Panels (a), (b) - The dispersion relation is reported as a function of the network Laplacian eigenvalues $\Lambda^{(\alpha)}$ (red dots), the blue curve is represented to emphasize the linear dependence: (a) stable regime $\lambda(\Lambda^{(\alpha)}) < 0$ for all α ; (b) unstable regime, there exist $\Lambda^{(\alpha)}$ associated to a positive dispersion relation, returning thus Turing pattern formation. Panels (c), (d) - Temporal evolution of $\xi_j(t)$ across nodes: (c) convergence to the homogeneous equilibrium of the oscillators in the stable regime; (d) Turing patterns emerge in the unstable regime. Panels (e), (f) - Network visualizations with node colors indicating dynamical states, values of $\xi_j(t)$ after a sufficiently long time: (e) nodes present the same color, meaning that oscillators assume the same value; (f) nodes present different colors indicating that in the unstable regime, Turing patterns emerge, i.e., ξ_j vary from node to node. The model parameters are $\sigma = -1 - 0.5i$, $\beta = 1 + i$, $\mu = 2 + 5.5i$ for the top panels (a), (c), and (e), while $\mu = -0.12 + 5.5i$ for the bottom panels (b), (d), and (f). The underlying topology is given by a stochastic block model of Erdős-Rényi network composed by $n = 50$ nodes and with $p_{in} = 0.6$ and $p_{out} = 0.02$, and $K = 4$ blocks.

where we used the definition of $z^{(s)}$, hence

$$\text{Re} \left[f'(z^{(s)}) \right] = -k\sigma_{\text{Re}}, \quad (45)$$

and being $k \geq 3$, stability occurs if $\sigma_{\text{Re}} > 0$, condition that we hereby assume to hold true.

Let us observe that Eq. (42) is invariant by rotation of a angle $2\pi/k$, indeed if we replace z_j by $z_j e^{i2\pi/k}$ then we obtain

$$e^{-i2\pi/k} \frac{dz_j}{dt} = \sigma e^{-i2\pi/k} z_j + \beta e^{-i2\pi(k+1)/k} (z_j)^{k+1}, \quad (46)$$

from which we can conclude

$$\frac{dz_j}{dt} = \sigma z_j + \beta z_j^{k+1}, \quad (47)$$

namely the original system.

Fix $s \in \{1, \dots, k\}$. We are now interested in studying the stability of the solution $z_j = z^{(s)}$ for all $j = 1, \dots, n$,

for the coupled system (41). We then introduce $z_j = z^{(s)} + u_j$, where $u_j \in \mathbb{C}$ is a small perturbation, and we perform a first-order expansion of Eq. (41):

$$\begin{aligned} \frac{du_j}{dt} &= \sigma u_j + \beta(k+1)(z^{(s)})^k u_j - \varepsilon \sum_{\ell} \mathcal{L}_{j\ell} u_{\ell} \\ &= -k\sigma u_j - \varepsilon \sum_{\ell} \mathcal{L}_{j\ell} u_{\ell}. \end{aligned} \quad (48)$$

By resorting again to the “rotated” variables, $\vec{w} = \mathcal{S}\vec{u}$, and by projecting them onto the supra-Laplace eigenbasis, we obtain:

$$\frac{d\hat{w}_{\alpha}}{dt} = \left[-k\sigma - \varepsilon \Lambda^{(\alpha)} \right] \hat{w}_{\alpha}; \quad (49)$$

the equilibrium solution $z_j = z^{(s)}$ is unstable if there exists $\alpha \geq 2$ such that

$$-k\sigma_{\text{Re}} - \varepsilon_{\text{Re}} \Lambda^{(\alpha)} > 0, \quad (50)$$

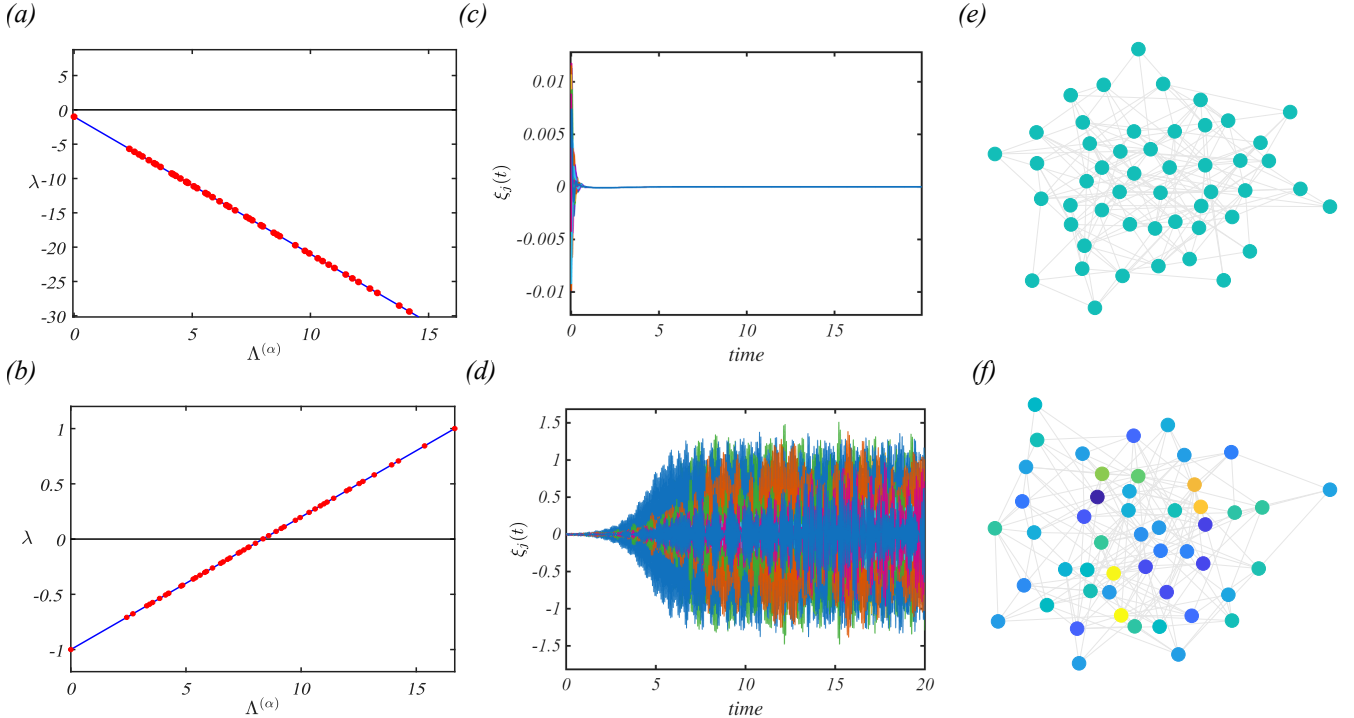


FIG. 2: Emergence of Turing patterns in a MWN with random Erdős–Rényi topology of coupled Stuart–Landau systems. Panels (a), (b) - Dispersion relations is shown as a function of the network Laplacian eigenvalues $\Lambda^{(\alpha)}$ (red dots), the blue curve is displayed to emphasize the linear dependence: (a) stable regime with a negative dispersion relation for all eigenvalues; (b) unstable regime with dispersion relation assuming positive values for some eigenvalues, Turing pattern can thus develop. Panels (c), (d) - Temporal evolution of $\xi_j(t)$ across nodes: (c) convergence to the homogeneous solution in the stable regime; (d) Turing patterns emerge in the unstable regime. Panels (e), (f) - Network visualizations with node colors indicating dynamical states, i.e., value of $\xi_j(t)$ after a sufficiently long time: (e) nodes present the same color, meaning that oscillators assumed the same value independently from the node index; (f) nodes present different colors indicating that in the unstable regime, Turing patterns emerge, i.e., nodes differentiate among themselves. The model parameters are $\sigma = -1 - 0.5i$, $\beta = 1 + i$, $\mu = 2 + 5.5i$ for the top panels (a), (c), and (e), while $\mu = -0.12 + 5.5i$ for the bottom panels (b), (d), and (f). The underlying topology is given by a Erdős–Rényi network composed by $n = 50$ nodes and $p = 0.15$.

namely

$$\varepsilon_{\text{Re}} < -k \frac{\sigma_{\text{Re}}}{\Lambda^{(\alpha)}}. \quad (51)$$

In Fig. 3, we report two cases supporting the analytical findings. In the former one, the coupling parameter ε does not satisfy condition (51) for any α and thus patterns cannot emerge (see top panels). On the other hand, in the second case, there exist several α such that condition (51) holds true for the chosen ε , and Turing patterns can emerge (see bottom panels). In both cases, the MWN is built by using a Barabári-Albert network composed by $n = 50$ nodes where at each step a single link and a single node are added. The MWN is coherent because the matrix weights have been built according to Proposition 1, where the matrices \mathbf{Q}_j are rotations by $2\pi/k$ with probability q or the identity matrix with probability $1 - q$; for this example we chosen $q = 1/2$. In this way, we can ensure that the dynamical system preserves

the coherence condition.

Finally, let us observe that the results of Fig. 3 have been obtained by using the variables “rotated” by the matrix \mathcal{S} , i.e., $\xi_j = \text{Re}(w_j)$, and this choice is mandatory; indeed by looking at the results in the original variables can be misleading: one can observe a heterogeneous solution even once the dispersion relation is negative (see Fig. 4), this is because of the mixing property induced by the transformations \mathbf{R}_{ij} that is removed once we use the rotated variables.

C. The Lorenz model

In the previous sections, we have considered one-dimensional complex systems (two-dimensional ones once we introduce real variables). The aim of this section is to provide an example in three dimensions. We hence consider a system of Lorenz oscillators, which provides

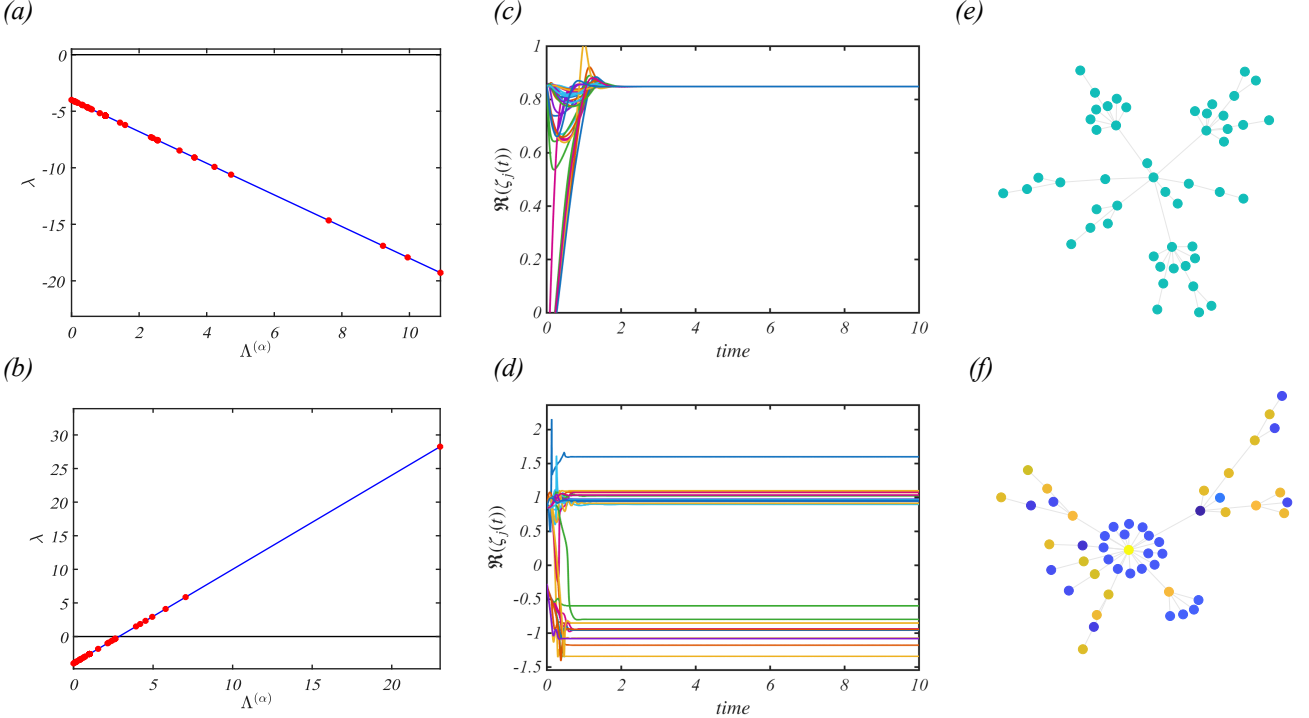


FIG. 3: **Emergence of Turing patterns for the abstract model (41) defined on top of a MWN whose underlying topology is given by a Barabási-Albert network composed by $n = 50$ nodes.** Panels (a), (b) - Dispersion relations as a function of the Laplace eigenvalues $\Lambda^{(\alpha)}$ (red dots), the blue curve has been drawn to help the reader and can be obtained by replacing the eigenvalues with a continuous variable. In panel (a), the dispersion relation remains negative for any value of $\Lambda^{(\alpha)}$, which prevents the emergence of Turing patterns, as can be observed in panel (c), where we report the time evolution of $\text{Re}(\zeta_j(t))$, and in panel (e) where we show the network whose nodes are colored according to the asymptotic stationary values of $\text{Re}(\zeta_j(t))$. In panel (b), we report the dispersion relations and we can observe that it assumes positive values (red dots) for some $\Lambda^{(\alpha)} \gtrsim 3$, Turing patterns can thus emerge as visible in panel (d), where we report $\text{Re}(\zeta_j(t))$ versus time and panels (f), where the network is displayed with the nodes again colored according to the asymptotic stationary values of $\text{Re}(\zeta_j(t))$. The model parameters are $k = 4$, $\sigma = 1 + i$, $\beta = 1 - 2i$, $\varepsilon = 1.4 + 2i$ for the top panels (a), (c), and (d), while $\varepsilon = -1.4 + 2i$ for the bottom panels (b), (d), and (f).

a canonical example of a three-dimensional nonlinear dynamical system exhibiting rich bifurcation scenarios. Unlike the two-dimensional Stuart-Landau system, the Lorenz system requires a three-dimensional state space and possesses multiple equilibria.

We now consider n copies of the Lorenz system coupled through a MWN, described by

$$\frac{d\vec{x}_j}{dt} = \vec{f}(\vec{x}_j) - \varepsilon \sum_{\ell} \mathcal{L}_{j\ell} \mathbf{E} \vec{x}_{\ell}, \quad (52)$$

where $\vec{x}_j = (x_j, y_j, z_j)^{\top}$ represents the state of oscillator j , \vec{f} is the Lorenz vector field, namely

$$\vec{f}(\vec{x}_j) = \begin{pmatrix} \sigma(y_j - x_j) \\ x_j(\rho - z_j) - y_j \\ x_j y_j - \beta z_j \end{pmatrix}, \quad (53)$$

$\varepsilon > 0$ is the coupling strength, \mathcal{L} is the supra-Laplace matrix, and $\mathbf{E} \in \mathbb{R}^{3 \times 3}$ describes how the dynamical variables

are coupled. Note that according to Turing's theory, the equilibrium under consideration must be stable. For $\rho > 1$, the uncoupled Lorenz system admits three equilibria: the origin and two symmetric non-trivial states

$$\vec{x}_{\pm}^* = \begin{pmatrix} \pm \sqrt{\beta(\rho - 1)} \\ \pm \sqrt{\beta(\rho - 1)} \\ \rho - 1 \end{pmatrix}. \quad (54)$$

In the following, we will consider $\vec{x}^* = \vec{x}_+^*$, that results stable if $\sigma > \beta + 1$ and $1 < \rho < \rho_H := \frac{\sigma(\sigma + \beta + 3)}{\sigma - \beta - 1}$.

Following Proposition 1, we construct a coherent MWN, in such a way that the three-dimensional Lorenz system is invariant with respect to the link transformations, i.e., the rotations. To achieve this goal, we associate with each node $i = 1, \dots, n$ an orthogonal matrix $\mathbf{R}_i \in O(3)$. By exploiting the symmetry properties of the Lorenz dynamics, we choose these matrices to have a block-diagonal structure: a 2×2 orthogonal block acting on the (x, y) -subspace and a unit entry in the $(3, 3)$

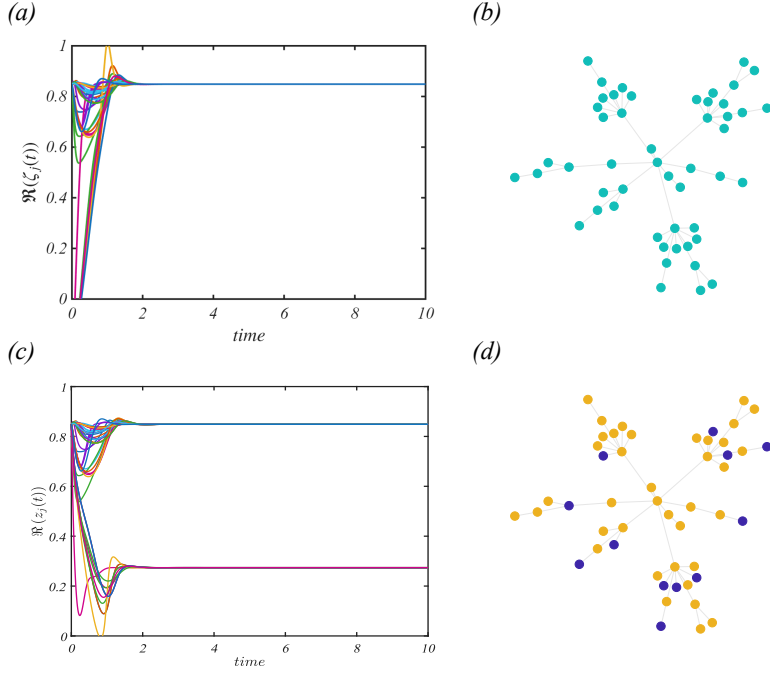


FIG. 4: **On the use of the rotated variables and the original ones.** We consider the model (41) with $k = 4$ defined on top of a MWN whose underlying topology is given by a Barabási-Albert network composed of $n = 50$ nodes. The parameters have been fixed so as to have a negative dispersion relation, $\sigma = 1 + i$, $\beta = 1 - 2i$, and $\varepsilon = 1.4 + 2i$. Hence, patterns cannot emerge as clearly shown in the top panels: (a) the time evolution of $\text{Re}(\zeta_j(t))$, and (b) the network with nodes colored according to the asymptotic values of $\text{Re}(\zeta_j(t))$. In the bottom panels, we show the same results but by using the original variables, (c) the time evolution of $\text{Re}(z_j(t))$, and (d) the network with nodes colored according to the asymptotic values of $\text{Re}(z_j(t))$. In both cases, a heterogeneous solution appears.

position.

Each matrix \mathbf{R}_i is randomly selected among two matrices which leave the function \vec{f} unchanged, namely, the identity matrix \mathbf{I}_3 and the reflection matrix $\mathbf{R}_\pi = \begin{pmatrix} -1 & 0 & 0 \\ 0 & -1 & 0 \\ 0 & 0 & 1 \end{pmatrix}$, both occurring with equal probability $q = 1/2$. The key property is that $\mathbf{R}_\pi \vec{f}(\mathbf{R}_\pi \vec{x}) = \vec{f}(\vec{x})$, $\forall \vec{x}$, ensuring invariance of the dynamics. For every pair of connected nodes (i, j) , we then construct matrix-valued edge weights so that the interaction between nodes i and j is weighted by the relative orthogonal transformation $\mathbf{R}_{ij} = \mathbf{R}_i^\top \mathbf{R}_j$. These matrix-valued weights are embedded into a supra-adjacency matrix $\mathcal{W} \in \mathbb{R}^{nd \times nd}$, where each nonzero block corresponds to the matrix \mathbf{R}_{ij} , the amplitudes w_{ij} , all reduced to unity for simplicity's sake.

Unlike the Stuart-Landau case, for the Lorenz system, the emergence of Turing instability relies on the study of the roots of a third-order polynomial. We could have used the explicit formula for the latter; however, we preferred to resort to the Routh-Hurwitz criterion (see Remark 2) and to numerical computations to analyze the dispersion relation.

Let us linearize Eq. (52) around its heterogeneous solution $\vec{X}^* = \mathcal{S}^\top (\vec{1}_n \otimes \vec{x}^*)$, where $\vec{x}^* = \vec{x}_+^*$ is given in Eq. (54), and by denoting with $\delta\vec{x}_j = \vec{x}_j - \vec{X}^*$ the perturbation of node j . By performing a first-order expansion,

we get

$$\frac{d\delta\vec{x}_j}{dt} = \mathbf{J}_f(\mathbf{O}_{1j}^\top \vec{x}^*) \delta\vec{x}_j - \varepsilon \sum_\ell \mathcal{L}_{j\ell} \mathbf{J}_h(\mathbf{O}_{1\ell}^\top \vec{x}^*) \delta\vec{x}_\ell \quad (55)$$

where $\delta\vec{x} = (\delta x^\top, \delta y^\top, \delta z^\top)^\top$ and $\mathbf{J}_f(\vec{x}^*)$, $\mathbf{J}_h(\vec{x}^*)$ are respectively the Jacobian of \vec{f} and $\vec{h}(\vec{x}) \equiv \mathbf{E}\vec{x}$ evaluated on the solution \vec{x}^* . By exploiting the invariance of the functions \vec{f} and $\mathbf{E}\vec{x}$, we can introduce the new “rotated” variables $\delta\vec{w}_j = \mathbf{O}_{1j} \delta\vec{x}_j$ and obtain

$$\frac{d\delta\vec{w}_j}{dt} = \mathbf{J}_f(\vec{x}^*) \delta\vec{w}_j - \varepsilon \sum_\ell \bar{\mathcal{L}}_{j\ell} \mathbf{E} \delta\vec{w}_\ell, \quad (56)$$

Let us now project the perturbation $\delta\vec{w}_j$ onto the eigenbasis of the Laplace matrix $\bar{\mathbf{L}}$ i.e., $\delta\vec{w}_j = \sum_\alpha \hat{w}_\alpha \phi_j^{(\alpha)}$. By inserting the latter into (56), one gets

$$\frac{d\hat{w}_\alpha}{dt} = (\mathbf{J}_f - \varepsilon \Lambda^{(\alpha)} \mathbf{E}) \hat{w}_\alpha, \quad (57)$$

where

$$\mathbf{J}_f = \begin{pmatrix} -\sigma & \sigma & 0 \\ \rho - z^* & -1 & -x^* \\ y^* & x^* & -\beta \end{pmatrix}. \quad (58)$$

It follows that the stability of the equilibrium \vec{X}^* can therefore be deduced by computing the eigenvalues of the matrices

$$\mathbf{M}(\Lambda^{(\alpha)}) = \mathbf{J}_f - \varepsilon \Lambda^{(\alpha)} \mathbf{E}. \quad (59)$$

In particular, a diffusion-driven instability occurs when the real part of at least one eigenvalue of $\mathbf{M}(\Lambda^{(\alpha)})$ becomes positive for some $\alpha > 1$. The characteristic equation associated with the latter matrix results to be a third-order polynomial that moreover depends on several model parameters. So instead of using the explicit formula for the third-order roots, we preferred to use a somewhat weaker result, but sufficient for our goal, which allows us to determine the sign of the root, namely the Routh-Hurwitz criterion.

Remark 2 (Routh–Hurwitz criterion for cubic polynomials). *Consider a monic cubic polynomial*

$$p(\lambda) = \lambda^3 + a_2 \lambda^2 + a_1 \lambda + a_0, \quad a_i \in \mathbb{R}. \quad (60)$$

All roots of p have strictly negative real part if and only if the following Routh–Hurwitz conditions are satisfied:

$$a_2 > 0, \quad a_1 > 0, \quad a_0 > 0, \quad a_2 a_1 > a_0. \quad (61)$$

As a first application, we will hereby show that if the coupling matrix \mathbf{E} has all zero elements but the diagonal ones, then Turing patterns cannot emerge. Indeed, in this case, we have

$$\mathbf{M}(\Lambda^{(\alpha)}) = \mathbf{J}_f - \varepsilon \Lambda^{(\alpha)} \begin{pmatrix} e_1 & 0 & 0 \\ 0 & e_2 & 0 \\ 0 & 0 & e_3 \end{pmatrix}, \quad (62)$$

with $e_j \in \{0, 1\}$. Hence the eigenvalues $\mu_j(\Lambda^{(\alpha)})$, $j = 1, 2, 3$, of $\mathbf{M}(\Lambda^{(\alpha)})$ are given by

$$\mu_j(\Lambda^{(\alpha)}) = \mu_j(0) - \varepsilon \Lambda^{(\alpha)} e_j, \quad (63)$$

where $\mu_j(0)$ are the eigenvalues of \mathbf{J}_f . By assumption, the equilibrium \vec{x}^* is stable, thus the latter has a negative real part and so do $\mu_j(\Lambda^{(\alpha)})$ for all α and $j = 1, 2, 3$.

In Fig. 5 we report numerical results supporting this finding. We consider a set of $n = 50$ Lorenz systems coupled through a random Erdős–Rényi MWN, with a probability of occurrence of a link between two nodes i and j equal to $p = 0.15$. The model parameters have been set to $\sigma = 13$, $\beta = 8$, and $\rho = 28$, ensuring the stability of the equilibrium point \vec{x}^* once the coupling is silenced. Top panels of Fig. 5 refer to the linear coupling $E_{11} = 1$ and $\varepsilon = 4$. As predicted by the analysis presented above, the dispersion relation is always negative (see panel (a)) and thus Turing instability does not hold, i.e., the equilibrium $\vec{x}_j = \vec{x}^*$ for all $j = 1, \dots, n$, remains stable also in presence of the coupling (see panel (c), where we plot the variable $\xi_j(t)$, i.e., the first component of the vector $\delta \vec{w}_j$) and state variables converge to the same value for all the nodes (see panel (e)).

Let us, now, consider a second case where the coupling mixes two different variables; for the sake of definiteness, we here consider $E_{31} = 1$ and the remaining entries of \mathbf{E} do vanish (the interested reader could find in Appendix C the analysis for all the remaining cases). The characteristic polynomial of $\mathbf{M}(\Lambda^{(\alpha)})$ Eq. (59), has coefficients

$$\begin{aligned} a_2 &= \sigma + \beta + 1, \\ a_1 &= \beta(\rho + \sigma), \\ a_0 &= 2\sigma\beta(\rho - 1) - \gamma\sigma\sqrt{\beta(\rho - 1)}, \end{aligned} \quad (64)$$

where we introduced $\gamma = \varepsilon \Lambda^{(\alpha)}$ to lighten the notations. The first two conditions (61) are trivially satisfied because of the positivity of the parameters. The necessary conditions for the emergence of Turing patterns are thus $a_0 < 0$ or $a_2 a_1 - a_0 < 0$. The former one is equivalent to

$$2\beta(\rho - 1) < \gamma\sqrt{\beta(\rho - 1)}, \quad (65)$$

that requires (see Appendix C for the detailed computation of $\gamma_{31}^{(crit)}$)

$$\varepsilon \Lambda^{(\alpha)} > 2\sqrt{\beta(\rho - 1)} = \gamma_{31}^{(crit)}. \quad (66)$$

Hence, if $\rho \geq 1$, one can obtain $a_0 < 0$ if $\Lambda^{(\alpha)}$ is sufficiently large.

Let us now consider the remaining case $a_2 a_1 - a_0 < 0$. A straightforward computation returns

$$\gamma\sigma\sqrt{\beta(\rho - 1)} - 2\beta\sigma(\rho - 1) + \beta(\rho + \sigma)(\beta + \sigma + 1) < 0, \quad (67)$$

which enables us to obtain

$$\varepsilon \Lambda^{(\alpha)} < 2\sqrt{\beta(\rho - 1)} - \frac{\beta(\rho + \sigma)(\beta + \sigma + 1)}{\sigma\sqrt{\beta(\rho - 1)}} = \gamma_2. \quad (68)$$

Let us however observe (see Appendix C) that $\gamma_2 < 0$ and thus condition (68) is never verified, being $\Lambda^{(\alpha)} \geq 0$. In conclusion Turing instability arises if condition (66) holds true.

In the bottom panels of Fig. 5, we show numerical results confirming the analytical ones. We consider again $n = 50$ Lorenz systems coupled through a random Erdős–Rényi MWN, with a probability of occurrence of a link between two nodes i and j equal to $p = 0.15$. The homogeneous equilibrium point \vec{x}^* is stable, being $\varepsilon = 4$, $\sigma = 13$, $\beta = 8$, and $\rho = 28$. The coupling is realized by assuming, $E_{31} = 1$ and the remaining entries $E_{ij} = 0$. One can observe the existence of large enough eigenvalues, $\Lambda^{(\alpha)} \gtrsim 7.35 = \gamma_{31}^{(crit)}/\varepsilon$, for which the dispersion relation is positive (see red dots in panel (b)) and thus patterns do emerge (see panels (d) and (f) where we report, respectively, the time evolution of $\xi_j(t)$ and the value of the same variable after a sufficiently long time period).

Another numerical example supporting the analytical findings is shown in Fig. 6. In this case, the underlying structures are generated from a stochastic block model

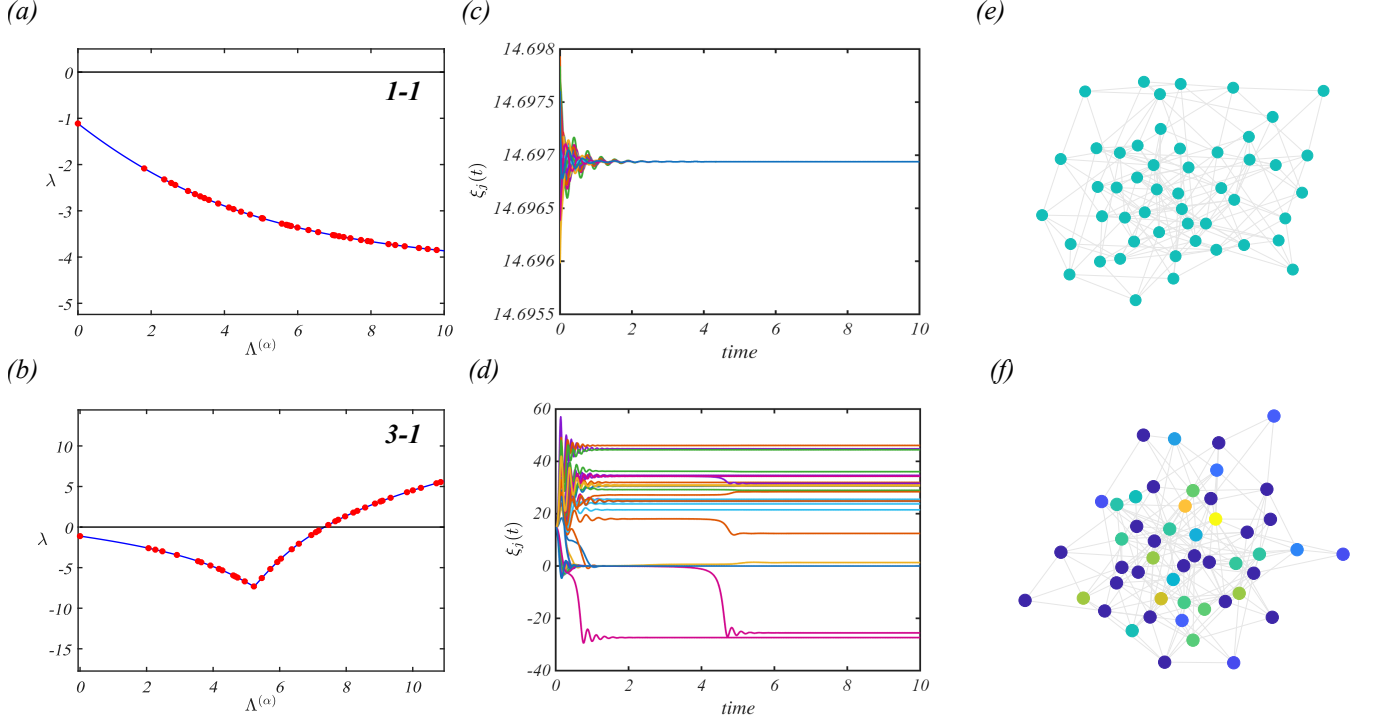


FIG. 5: Emergence of Turing patterns in a MWN with random Erdős–Rényi topology of coupled Lorenz systems. Panels (a), (b) - The dispersion relations is displayed as a function of network Laplacian eigenvalue $\Lambda^{(\alpha)}$ (reds dots), the blue curve have been obtained by replacing the latter with a continuous variable and it is shown to help the reader to appreciate the nonlinear behavior: (a) the dispersion relation remains negative for any value of $\Lambda^{(\alpha)}$, which prevents the emergence of Turing patterns; (b) negative dispersion relationship up to a critical threshold of $\Lambda^{(\alpha)}$, beyond which it becomes positive enabling the emergence of Turing patterns. Panels (c), (d) - Temporal evolution of $\xi_j(t)$ across nodes: (c) all variables $\xi_j(t)$ converge to the equilibrium point ξ^* ; (d) emergence of Turing patterns. Panels (e), (f) - Network visualizations with node colors indicating dynamical states, i.e., $\xi_j(t)$ after a sufficiently long period of time: (e) nodes present same color meaning that oscillators reached the same value regardless of the node index; (f) nodes present different colors indicating the onset of Turing patterns. The model parameters used to obtain the presented results are $\sigma = 13$, $\rho = 28$, $\beta = 8$. The underlying topology is given by a Erdős–Rényi network composed by $n = 50$ nodes and $p = 0.15$., and the coupling is obtained with $\varepsilon = 4$ and $E_{11} = 1$ (top panels) while $E_{31} = 1$ (bottom panels).

topology composed of $n = 50$ nodes divided into three blocks. The probability of forming a link between two nodes within the same block is set to $p_{\text{in}} = 0.8$, while the probability of forming a link between nodes belonging to different blocks is $p_{\text{out}} = 0.09$. The model parameters used in this example correspond to $\sigma = 13$, $\beta = 8$, and $\rho = 28$. Top panels of Fig. 6 refer to the linear coupling $E_{22} = 1$ and $\varepsilon = 4$. Once again, the dispersion relation is always negative (see panel (a)) and Turing patterns cannot emerge since the equilibrium $\vec{x}_j = \vec{x}^*$ for all $j = 1, \dots, n$, remains stable in presence of the coupling (see panel (c) and (e)). In the bottom panels, Numerical results are presented for $E_{23} = 1$ and $\varepsilon = 4$. One can observe the existence of eigenvalues $\Lambda^{(\alpha)} \gtrsim 6.08 = \gamma_{23}^{(\text{crit})}/\varepsilon$ (where $\gamma_{23}^{(\text{crit})}$ is given by Eq. (C15)) for which the dispersion relation is positive (see red dots in panel (b)) and thus patterns do emerge (see panels (d) and (f)).

V. CONCLUSIONS

In this work, we have explored the phenomenon of diffusion-driven instabilities in Matrix-Weighted Networks (MWNs), a recently introduced framework in which the modeling of interactions between node variables relies on matrix weights that encode both interaction strength and directional transformations. Our study has extended the classical theory of Turing pattern formation, originally formulated for systems coupled via scalar-weighted edges, to this more general setting.

A key notion in our analysis is *coherence*, a structural property of MWNs that ensures the composition of transformation matrices along any oriented cycle equals the identity. As also established in the context of global synchronization [30], we have shown that coherence is a necessary condition for the emergence of Turing instabilities in MWNs. Indeed, only when the MWN is coherent, one

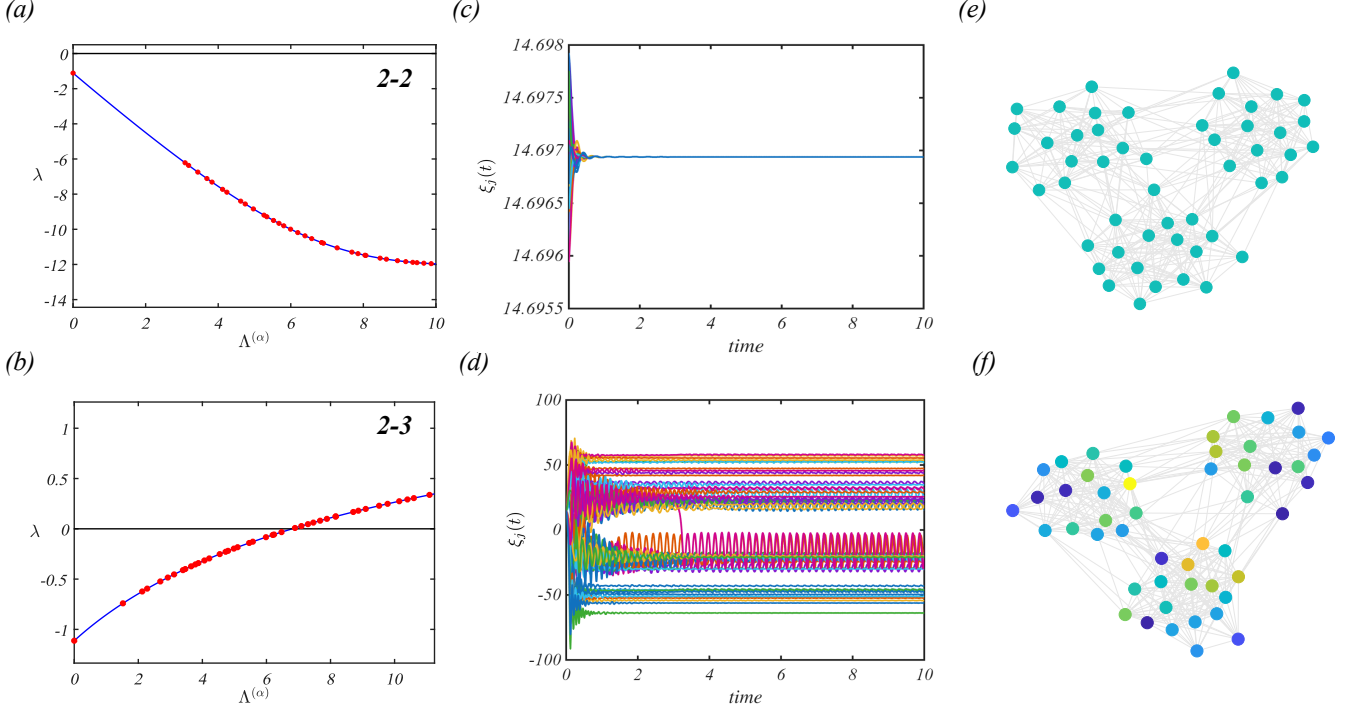


FIG. 6: Emergence of Turing patterns in a MWN with stochastic block model topology of coupled Lorenz systems. Panels (a), (b) - The dispersion relations is displayed as a function of network Laplacian eigenvalue $\Lambda^{(\alpha)}$ (red dots), the blue curve have been obtained by replacing the latter with a continuous variable and it is shown to help the reader to appreciate the nonlinear behavior: (a) the dispersion relation remains negative for any value of $\Lambda^{(\alpha)}$, which prevents the emergence of Turing patterns; (b) negative dispersion relationship up to a critical threshold of $\Lambda^{(\alpha)}$, beyond which it becomes positive enabling the emergence of Turing patterns. Panels (c), (d) - Temporal evolution of $\xi_j(t)$ across nodes: (c) all variables $\xi_j(t)$ converge to the equilibrium point ξ^* ; (d) emergence of Turing patterns. Panels (e), (f) - Network visualizations with node colors indicating dynamical states, i.e., $\xi_j(t)$ after a sufficiently long period of time: (e) nodes present same color meaning that oscillators assume the same value; (f) nodes present different colors indicating the onset of Turing patterns. The model parameters used to compute the dynamics are $\sigma = 13$, $\rho = 28$, $\beta = 8$. The underlying topology is given by a stochastic bloc model of Erdős–Rényi network composed by $n = 50$ nodes and with $p_{in} = 0.8$ and $p_{out} = 0.09$. The coupling is obtained with $\varepsilon = 4$, $E_{22} = 1$ (top panels) and $E_{23} = 1$ bottom panels).

can disentangle the mix of variables created by the transformation weights via the matrix \mathcal{S} ; the latter allows us to reduce the supra-Laplacian \mathcal{L} to a scalar Laplacian $\tilde{\mathcal{L}} = \mathcal{S}\mathcal{L}\mathcal{S}^\top$, whose spectral decomposition can be used to explain the instability analysis.

Furthermore, we have proposed a novel characterization of coherent MWNs, allowing us to deal with networks of any size and thus to overcome the limitation of the existing literature, where only small hand-made coherent networks have been considered. The proposed algorithm relies on the fact that link transformations can be rewritten as relative rotations between nodes; the method is thus very general and can open the way to many more applications of MWN.

Here, we have considered edge weights defined as rotation matrices, thereby imposing specific structural constraints on the class of admissible dynamical systems, namely, those invariant under the action of such matri-

ces. Notice that the proposed framework can be further generalized to include general orthogonal matrices by imposing additional constraints on the dynamical systems, namely, the invariance with respect to these matrices.

We have focused on the emergence of diffusion-driven instabilities by considering three different models, namely, the Stuart-Landau (SL) model, an abstract model invariant under $2\pi/k$ -rotations, and the Lorenz system. In the case of the SL model, the analysis was carried out analytically in closed form. Exploiting the rotational symmetry of the dynamics in the (x, y) -plane, we have showed that the dispersion relation reduces to a simple spectral condition on the Laplacian eigenvalues, yielding a sharp critical threshold $\Lambda_{\text{crit}} = -\sigma_{\text{Re}}/\mu_{\text{Re}}$: modes with $\Lambda^{(\alpha)} > \Lambda_{\text{crit}}$ become unstable, while the homogeneous mode remains stable. A similar result has been provided for the abstract model invariant under $2\pi/k$ rotations, and it has allowed us to explore the role of dis-

crete rotational symmetries of higher order in the pattern formation mechanism. Finally, for the Lorenz system, we have analytically proved that diagonal couplings can never lead to the emergence of Turing instability, regardless of the network topology. In contrast, we have proved that off-diagonal couplings admit a diffusion-driven instability for appropriate parameter regimes. In all three settings, all the analytical predictions were confirmed by numerical simulations.

Our finding reveals an interesting interplay between the MWN structure, encoded in its matrix weights and coherence properties, and the dynamical system. Such an interplay is absent in classical scalar-weighted networks and represents a genuinely new feature introduced by the MWN setting. For future investigation, it would be of interest to understand how the breaking of coherence affects the onset of pattern formation and whether

approximate coherence can still lead to instabilities.

AUTHOR CONTRIBUTIONS

A.G., W.S., and T.C. contributed equally to the project and the preparation of the manuscript.

CODE AVAILABILITY

The codes supporting the findings of this study are available from the authors upon request.

COMPETING INTERESTS

The authors declare no competing interests.

[1] P. W. Anderson, *Physical Review Letters* **177**, 4047 (1972).

[2] G. Nicolis and I. Prigogine, *Self-organization in nonequilibrium systems: From dissipative structures to order through fluctuations* (J. Wiley and Sons, 1977).

[3] R. Pastor-Satorras and A. Vespignani, *Nature Physics* **6**, 480 (2010).

[4] A. M. Turing, *Phil. Trans. R. Soc. Lond. B* **237**, 37 (1952).

[5] J. D. Murray, *Mathematical biology II: Spatial models and biomedical applications* (Springer-Verlag, 2001).

[6] H. Nakao and A. S. Mikhailov, *Nature Physics* **6**, 544 (2010).

[7] M. Asllani, J. Challenger, F. Pavone, L. Sacconi, and D. Fanelli, *Nature Communications* **5**, 4517 (2014).

[8] M. Asllani and T. Carletti, *Physical Review E* **97**, 042302 (2018).

[9] R. Muolo, M. Asllani, D. Fanelli, P. Maini, and T. Carletti, *Journal Theoretical Biology* **480**, 81 (2019).

[10] M. Asllani, D. Busiello, T. Carletti, D. Fanelli, and G. Planchon, *Phys. Rev. E* **90**, 042814 (2014).

[11] N. Kouvaris, S. Hata, and A. Diaz-Guilera, *Sci. Rep.* **5**, 10840 (2015).

[12] D. Busiello, T. Carletti, and D. Fanelli, *Eur. Phys. Letters* **121**, 48006 (2018).

[13] F. Battiston, G. Cencetti, I. Iacopini, V. Latora, M. Lucas, A. Patania, J. Young, and G. Petri, *Phys. Rep.* **874**, 1 (2020).

[14] S. Boccaletti, P. De Lellis, C. del Genio, K. Alfar-Bittner, R. Criado, S. Jalan, and M. Romance, *Physics Reports* **1018**, 1 (2023), the structure and dynamics of networks with higher order interactions.

[15] Z. Gao, D. Ghosh, H. A. Harrington, J. G. Restrepo, and D. Taylor, *Chaos: An Interdisciplinary Journal of Nonlinear Science* **33**, 040401 (2023).

[16] F. Battiston, E. Amico, A. Barrat, G. Bianconi, G. de Arruada, B. Franceschiello, I. Iacopini, S. Kéfi, V. Latora, Y. Moreno, M. Murray, T. Peixoto, F. Vaccarino, and G. Petri, *Nature Physics* **1018**, 1 (2023).

[17] A. P. Millán, H. Sun, L. Giambagli, R. Muolo, T. Carletti, J. J. Torres, F. Radicchi, J. Kurths, and G. Bianconi, *Nature Physics* **21**, 353 (2025).

[18] T. Carletti, D. Fanelli, and S. Nicoletti, *J. Phys. Complex.* **1**, 035006 (2020).

[19] S. Gao, L. Chang, M. Perc, and Z. Wang, *Phys. Rev. E* **107**, 014216 (2023).

[20] R. Muolo, L. Gallo, V. Latora, M. Frasca, and T. Carletti, *Chaos, Solitons & Fractals* **166** (2023).

[21] M. Dorchain, W. Segnou, R. Muolo, and T. Carletti, *Chaos, Solitons & Fractals* **189**, 115730 (2024).

[22] L. Giambagli, M. Calmon, R. Muolo, T. Carletti, and G. Bianconi, *Phys. Rev. E* **106**, 064314 (2022).

[23] R. Muolo, T. Carletti, and G. Bianconi, *Chaos, Solitons & Fractals* **178**, 114312 (2024).

[24] R. Muolo, L. Giambagli, H. Nakao, D. Fanelli, and T. Carletti, *Proceedings of the Royal Society A: Mathematical, Physical and Engineering Sciences* **480**, 20240235 (2024).

[25] G. Gambino, M. Lombardo, and M. Sammartino, *Mathematics and Computers in Simulation* **82**, 1112 (2012), *nonlinear Waves: Computation and Theory-IX, WAVES 2009*.

[26] D. Fanelli, C. Cianci, and F. Di Patti, *Eur. Phys. J. B* **86**, 142 (2013).

[27] S. Gao, L. Chang, X. Wang, C. Liu, X. Li, and Z. Wang, *New Journal of Physics* **22**, 053047 (2020).

[28] C. Kuehn and C. Soresina, *Journal of Complex Networks* **12**, cnad052 (2024).

[29] Y. Tian, S. Kojaku, H. Sayama, and R. Lambiotte, *Physical Review Letters* **134**, 237401 (2025).

[30] A. Gallo, Y. Tian, R. Lambiotte, and T. Carletti, *Communications Physics* **8** (2025).

[31] F. Hirokazu and Y. Tomoji, *Progress of Theoretical Physics* **69**, 32 (1983).

[32] L. Pecora, T. Carroll, G. Johnson, D. Mar, and J. Heagy, *Chaos: An Interdisciplinary Journal of Nonlinear Science* **7**, 520 (1997).

- [33] L. Pecora and T. Carroll, *Physical Review Letters* **80**, 2109 (1998).
- [34] J. T. Stuart and R. C. DiPrima, *Proceedings of the Royal Society of London. A. Mathematical and Physical Sciences* **362**, 27 (1978).
- [35] A. van Harten, *Journal of Nonlinear Science* **1**, 397 (1991).
- [36] I. Aranson and L. Kramer, *Reviews of Modern Physics* **74**, 99 (2002).
- [37] V. Garca-Morales and K. Krischer, *Contemporary Physics* **53**, 79 (2012).

Appendix A: Characterization of coherent MWNs

This appendix is devoted to provide an in-depth analysis of the characterization of coherent MWNs proposed in Proposition 1. As in [29], we restrict our attention to reciprocal interactions. Accordingly, without loss of generality, we present the discussion in terms of undirected networks.

Lemma 3 (Coherence on a cycle basis). *Let $G = (V, E)$ be a MWN graph let $\mathcal{B} = \{\mathcal{C}_1, \dots, \mathcal{C}_\beta\}$ be a cycle basis of G . Assume that for every edge $(i, j) \in E$ the link matrix \mathbf{R}_{ij} is orthonormal. If*

$$\prod_{(i,j) \in \mathcal{C}_k} \mathbf{R}_{ij} = \mathbf{I}_d, \quad \forall \mathcal{C}_k \in \mathcal{B}, \quad (\text{A1})$$

then

$$\prod_{(i,j) \in \mathcal{C}} \mathbf{R}_{ij} = \mathbf{I}_d \quad (\text{A2})$$

for any cycle \mathcal{C} in G .

Proof. Since \mathcal{B} is a cycle basis, it follows that any cycle \mathcal{C} of G can be written as the symmetric difference of a finite number of cycles in \mathcal{B} , i.e., $\mathcal{C} = \mathcal{C}_{k_1} \oplus \dots \oplus \mathcal{C}_{k_m}$. Notice that each edge (i, j) that appears twice in the symmetric difference corresponds to the factor $\mathbf{R}_{ij} \mathbf{R}_{ji}$ in the ordered product; hence, since \mathbf{R}_{ij} is orthonormal, $\mathbf{R}_{ij}^{-1} = \mathbf{R}_{ji}$, and the corresponding factor cancels out in the ordered product.

By assumption, Eq. (A1) holds, i.e., the product of link matrices along each cycle $\mathcal{C}_k \in \mathcal{B}$ equals the identity matrix. Therefore, the product along \mathcal{C} also equals the identity. \square

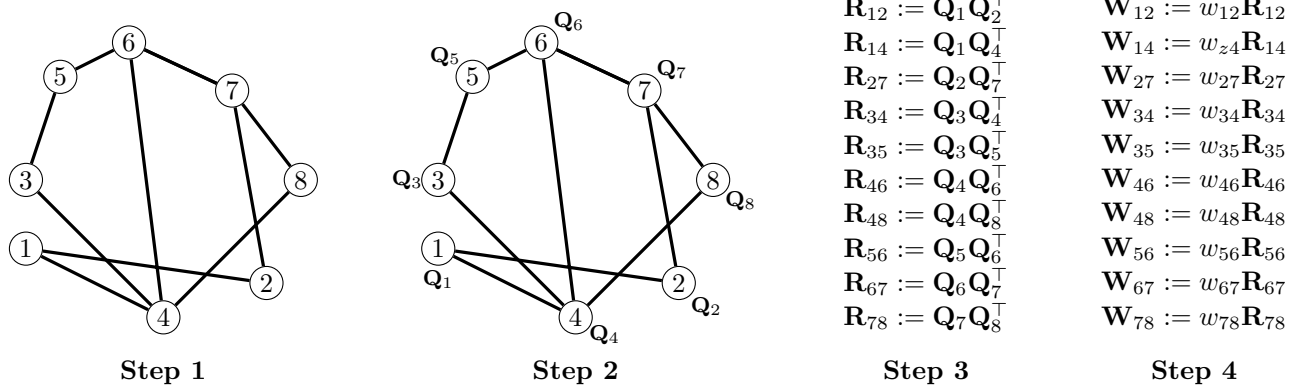


FIG. 7: **Construction of a coherent MWNs.** **Step 1:** generate underlying topology. **Step 2:** assign a $d \times d$ orthonormal matrix $\mathbf{Q}_i \in O(d)$ to each node. **Step 3:** For each edge, define the transformation matrix as the product of the orthonormal matrix of an endpoint and the transpose of the other one. **Step 4:** For each edge, define the corresponding weighted matrix as the product between a scalar weight $w_{ij} \in U[w_{\min}, w_{\max}]$ and the corresponding transformation matrix.

Let us discuss the illustrative example in Fig. 8. A cycle basis \mathcal{B} of the graph G in Fig. 8(a) is given by the three cycles shown separately in fig 8(b):

- $\mathcal{C}_1 = (3, 5, 6, 4, 3)$;
- $\mathcal{C}_2 = (4, 6, 7, 8, 4)$;
- $\mathcal{C}_3 = (1, 2, 7, 6, 4, 1)$.

Indeed, notice that we can write the remaining cycles $\mathcal{C}_4, \mathcal{C}_5$ and \mathcal{C}_6 in terms of such a basis:

- $\mathcal{C}_4 = (1, 2, 7, 8, 4, 1) = \mathcal{C}_2 \oplus \mathcal{C}_3 = (\mathcal{C}_2 \cup \mathcal{C}_3) \setminus (\mathcal{C}_2 \cap \mathcal{C}_3)$;
- $\mathcal{C}_5 = (3, 4, 8, 7, 6, 5, 3) = \mathcal{C}_1 \oplus \mathcal{C}_2 = (\mathcal{C}_1 \cup \mathcal{C}_2) \setminus (\mathcal{C}_1 \cap \mathcal{C}_2)$;

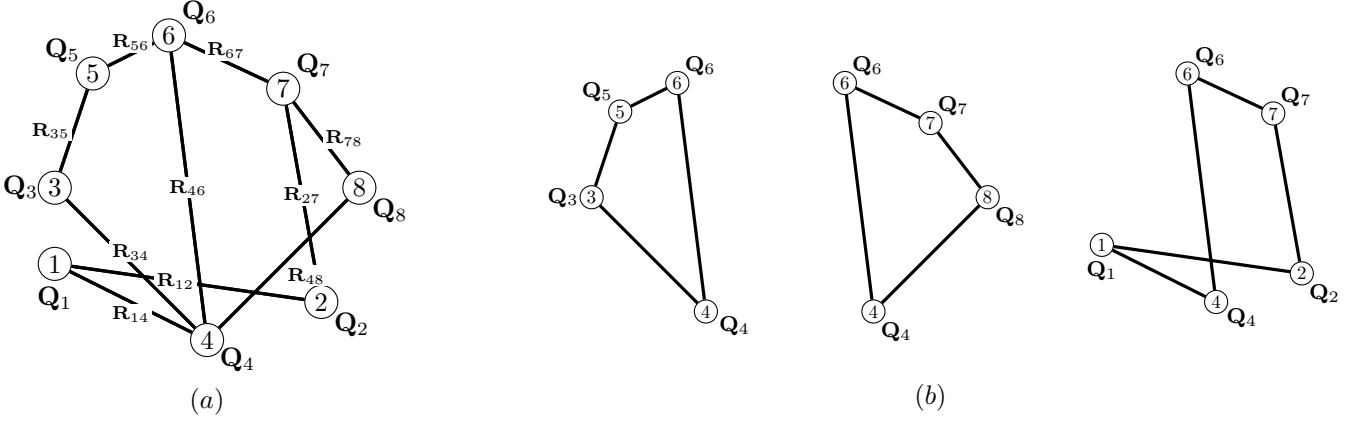


FIG. 8: Panel (a) - **Coherent MWN G defined in Fig. 7.** G has six distinct cycles, i.e., $\mathcal{C}_1 = (3, 5, 6, 4, 3)$, $\mathcal{C}_2 = (4, 6, 7, 8, 4)$, $\mathcal{C}_3 = (1, 2, 7, 6, 4, 1)$, $\mathcal{C}_4 = \{1, 2, 7, 8, 4, 1\}$, $\mathcal{C}_5 = \{3, 4, 8, 7, 6, 5, 3\}$ and $\mathcal{C}_6 = \{1, 2, 7, 6, 5, 3, 4, 1\}$. Panel (b) - **Cycle basis \mathcal{B} of G .**

- $\mathcal{C}_6 = (1, 2, 7, 6, 5, 3, 4, 1) = \mathcal{C}_1 \oplus \mathcal{C}_3 = (\mathcal{C}_1 \cup \mathcal{C}_3) \setminus (\mathcal{C}_1 \cap \mathcal{C}_3)$.

To verify the coherence condition, we need to check that the product of link matrices equals identity for each cycle $\mathcal{C}_1 = (3, 5, 6, 4, 3)$, $\mathcal{C}_2 = (4, 6, 7, 8, 4)$, and $\mathcal{C}_3 = (1, 2, 7, 6, 4, 1)$:

$$\begin{aligned} \mathcal{C}_1 : \quad \mathbf{R}_{35}\mathbf{R}_{56}\mathbf{R}_{64}\mathbf{R}_{43} &= (\mathbf{Q}_3^\top \mathbf{Q}_5)(\mathbf{Q}_5^\top \mathbf{Q}_6)(\mathbf{Q}_6^\top \mathbf{Q}_4)(\mathbf{Q}_4^\top \mathbf{Q}_3) \\ &= \mathbf{Q}_3^\top (\mathbf{Q}_5 \mathbf{Q}_5^\top)(\mathbf{Q}_6 \mathbf{Q}_6^\top)(\mathbf{Q}_4 \mathbf{Q}_4^\top) \mathbf{Q}_3 \\ &= \mathbf{Q}_3^\top \mathbf{Q}_3 = \mathbf{I}_d; \end{aligned} \quad (A3)$$

$$\begin{aligned} \mathcal{C}_2 : \quad \mathbf{R}_{46}\mathbf{R}_{67}\mathbf{R}_{78}\mathbf{R}_{84} &= (\mathbf{Q}_4^\top \mathbf{Q}_6)(\mathbf{Q}_6^\top \mathbf{Q}_7)(\mathbf{Q}_7^\top \mathbf{Q}_8)(\mathbf{Q}_8^\top \mathbf{Q}_4) \\ &= \mathbf{Q}_4^\top (\mathbf{Q}_6 \mathbf{Q}_6^\top)(\mathbf{Q}_7 \mathbf{Q}_7^\top)(\mathbf{Q}_8 \mathbf{Q}_8^\top) \mathbf{Q}_4 \\ &= \mathbf{Q}_4^\top \mathbf{Q}_4 = \mathbf{I}_d; \end{aligned} \quad (A4)$$

$$\begin{aligned} \mathcal{C}_3 : \quad \mathbf{R}_{12}\mathbf{R}_{27}\mathbf{R}_{76}\mathbf{R}_{64}\mathbf{R}_{41} &= (\mathbf{Q}_1^\top \mathbf{Q}_2)(\mathbf{Q}_2^\top \mathbf{Q}_7)(\mathbf{Q}_7^\top \mathbf{Q}_6)(\mathbf{Q}_6^\top \mathbf{Q}_4)(\mathbf{Q}_4^\top \mathbf{Q}_1) \\ &= \mathbf{Q}_1^\top (\mathbf{Q}_2 \mathbf{Q}_2^\top)(\mathbf{Q}_7 \mathbf{Q}_7^\top)(\mathbf{Q}_6 \mathbf{Q}_6^\top)(\mathbf{Q}_4 \mathbf{Q}_4^\top) \mathbf{Q}_1 \\ &= \mathbf{Q}_1^\top \mathbf{Q}_1 = \mathbf{I}_d. \end{aligned} \quad (A5)$$

By Lemma 3, coherence of \mathcal{B} implies coherence of all cycles in the graph.

Let us now consider the opposite direction of Proposition 1, i.e., given the coherent MWN G in Fig. 8 to each edge (i, j) to which an orthonormal matrix \mathbf{R}_{ij} is assigned, we show how to explicitly construct the orthonormal matrices $\mathbf{Q}_1, \dots, \mathbf{Q}_8 \in O(d)$ such that $\mathbf{R}_{ij} = \mathbf{Q}_i^\top \mathbf{Q}_j$ for any edge (i, j) .

First, let us choose a reference node in $V = \{1, \dots, 8\}$ and set an initial matrix. Without loss of generality, we select node $k = 4$ as the reference one and set $\mathbf{Q}_4 = \mathbf{I}_d$. Second, let us construct the orthonormal matrices to be assigned to the other nodes via paths from the reference node $k = 4$. For any $j \in V \setminus \{4\}$, we choose a path from node 4 to node j and define $\mathbf{Q}_j := \mathbf{Q}_4 \mathbf{R}_{P_{4j}} = \mathbf{R}_{P_{4j}}$. Explicitly, we then have:

- $P_{41} = (4, 1)$: $\mathbf{Q}_1 = \mathbf{R}_{41} = \mathbf{R}_{14}^\top$;
- $P_{42} = (4, 1, 2)$: $\mathbf{Q}_2 = \mathbf{R}_{41}\mathbf{R}_{12} = \mathbf{R}_{14}^\top \mathbf{R}_{12}$;
- $P_{43} = (4, 3)$: $\mathbf{Q}_3 = \mathbf{R}_{43} = \mathbf{R}_{34}^\top$;
- $P_{45} = (4, 3, 5)$: $\mathbf{Q}_5 = \mathbf{R}_{43}\mathbf{R}_{35} = \mathbf{R}_{34}^\top \mathbf{R}_{35}$;
- $P_{46} = (4, 6)$: $\mathbf{Q}_6 = \mathbf{R}_{46}$;
- $P_{47} = (4, 6, 7)$: $\mathbf{Q}_7 = \mathbf{R}_{46}\mathbf{R}_{67}$;
- $P_{48} = (4, 6, 7, 8)$: $\mathbf{Q}_8 = \mathbf{R}_{46}\mathbf{R}_{67}\mathbf{R}_{78}$.

Third, to conclude, let us verify that $\mathbf{R}_{ij} = \mathbf{Q}_i^\top \mathbf{Q}_j$ for any edge (i, j) .

For edge $(1, 2)$, we have

$$\mathbf{Q}_1^\top \mathbf{Q}_2 = (\mathbf{R}_{14}^\top)^\top \mathbf{R}_{14}^\top \mathbf{R}_{12} = \mathbf{R}_{14} \mathbf{R}_{14}^\top \mathbf{R}_{12} = \mathbf{R}_{12}. \quad (\text{A6})$$

For edge $(2, 7)$, we have:

$$\mathbf{Q}_2^\top \mathbf{Q}_7 = (\mathbf{R}_{14}^\top \mathbf{R}_{12})^\top \mathbf{R}_{46} \mathbf{R}_{67} = \mathbf{R}_{12}^\top \mathbf{R}_{14} \mathbf{R}_{46} \mathbf{R}_{67} = \mathbf{R}_{21} \mathbf{R}_{14} \mathbf{R}_{46} \mathbf{R}_{67} = \mathbf{R}_{27}, \quad (\text{A7})$$

where the last equality follows by the coherence condition on cycle \mathcal{C}_3 .

For edge $(5, 6)$, we have:

$$\mathbf{Q}_5^\top \mathbf{Q}_6 = (\mathbf{R}_{34}^\top \mathbf{R}_{35})^\top \mathbf{R}_{46} = \mathbf{R}_{35}^\top \mathbf{R}_{34} \mathbf{R}_{46} = \mathbf{R}_{56}, \quad (\text{A8})$$

where the last equality follows by the coherence condition on cycle \mathcal{C}_1 .

For edge $(3, 5)$, we have:

$$\mathbf{Q}_3^\top \mathbf{Q}_5 = (\mathbf{R}_{43})^\top \mathbf{R}_{34}^\top \mathbf{R}_{35} = \mathbf{R}_{34} \mathbf{R}_{34}^\top \mathbf{R}_{35} = \mathbf{R}_{35}. \quad (\text{A9})$$

For edge $(6, 7)$, we have:

$$\mathbf{Q}_6^\top \mathbf{Q}_7 = (\mathbf{R}_{46})^\top \mathbf{R}_{46} \mathbf{R}_{67} = \mathbf{R}_{64} \mathbf{R}_{46} \mathbf{R}_{67} = \mathbf{R}_{67}. \quad (\text{A10})$$

For edge $(7, 8)$, we have:

$$\mathbf{Q}_7^\top \mathbf{Q}_8 = (\mathbf{R}_{46} \mathbf{R}_{67})^\top \mathbf{R}_{46} \mathbf{R}_{67} \mathbf{R}_{78} = \mathbf{R}_{67}^\top \mathbf{R}_{46}^\top \mathbf{R}_{46} \mathbf{R}_{67} \mathbf{R}_{78} = \mathbf{R}_{78}. \quad (\text{A11})$$

Similarly, the proof also holds for the remaining edges $(1, 4)$, $(3, 4)$, $(4, 6)$ and $(4, 8)$. Notice that the coherence property ensures that this construction is well-defined, i.e., different path choices from node 4 to node j yield the same matrix \mathbf{Q}_j . For instance, if we consider the path $P'_{45} = (4, 6, 5)$, we could define $\tilde{\mathbf{Q}}_5 = \mathbf{R}_{46} \mathbf{R}_{65}$. Since from the coherence condition on cycle \mathcal{C}_1 we have that $\mathbf{R}_{46} \mathbf{R}_{65} \mathbf{R}_{53} \mathbf{R}_{34} = \mathbf{I}_d$, we conclude that

$$\tilde{\mathbf{Q}}_5 = \mathbf{R}_{46} \mathbf{R}_{65} = \mathbf{R}_{34}^\top \mathbf{R}_{53}^\top = \mathbf{R}_{34}^\top \mathbf{R}_{35} = \mathbf{Q}_5. \quad (\text{A12})$$

Appendix B: Linear stability analysis of the Stuart-Landau model

In this appendix, we present a detailed derivation of the linear stability of a network of Stuart-Landau (SL) oscillators, by including the conditions for diffusion-driven instabilities and the absence of stable limit cycles near the origin.

Let us consider n identical SL oscillators, whose dynamics are governed by

$$\frac{d}{dt} \begin{pmatrix} x \\ y \end{pmatrix} = \begin{pmatrix} \sigma_{\text{Re}} & -\sigma_{\text{Im}} \\ \sigma_{\text{Im}} & \sigma_{\text{Re}} \end{pmatrix} \begin{pmatrix} x \\ y \end{pmatrix} - (x^2 + y^2) \begin{pmatrix} \beta_{\text{Re}} & -\beta_{\text{Im}} \\ \beta_{\text{Im}} & \beta_{\text{Re}} \end{pmatrix} \begin{pmatrix} x \\ y \end{pmatrix}, \quad (\text{B1})$$

where $\sigma = \sigma_{\text{Re}} + i\sigma_{\text{Im}}$ and $\beta = \beta_{\text{Re}} + i\beta_{\text{Im}}$ are complex model parameters, and coupled by a diffusive-like nonlinear function

$$\vec{h}(x_\ell, y_\ell) := (x_\ell^2 + y_\ell^2)^{\frac{m-1}{2}} \begin{pmatrix} \mu_{\text{Re}} & -\mu_{\text{Im}} \\ \mu_{\text{Im}} & \mu_{\text{Re}} \end{pmatrix} \begin{pmatrix} x_\ell \\ y_\ell \end{pmatrix}, \quad (\text{B2})$$

with $\mu = \mu_{\text{Re}} + i\mu_{\text{Im}}$ being the complex coupling strength and $m \geq 1$ controlling the nonlinearity of the coupling. The evolution of the j -th oscillator is, thus, given by

$$\begin{aligned} \frac{d}{dt} \begin{pmatrix} x_j \\ y_j \end{pmatrix} &= \begin{pmatrix} \sigma_{\text{Re}} & -\sigma_{\text{Im}} \\ \sigma_{\text{Im}} & \sigma_{\text{Re}} \end{pmatrix} \begin{pmatrix} x_j \\ y_j \end{pmatrix} - (x_j^2 + y_j^2) \begin{pmatrix} \beta_{\text{Re}} & -\beta_{\text{Im}} \\ \beta_{\text{Im}} & \beta_{\text{Re}} \end{pmatrix} \begin{pmatrix} x_j \\ y_j \end{pmatrix} - \sum_\ell \mathcal{L}_{j\ell} \left[(x_\ell^2 + y_\ell^2)^{\frac{m-1}{2}} \begin{pmatrix} \mu_{\text{Re}} & -\mu_{\text{Im}} \\ \mu_{\text{Im}} & \mu_{\text{Re}} \end{pmatrix} \begin{pmatrix} x_\ell \\ y_\ell \end{pmatrix} \right] \\ &=: \vec{f}(x_j, y_j) - \sum_\ell \mathcal{L}_{j\ell} \vec{h}(x_\ell, y_\ell), \end{aligned} \quad (\text{B3})$$

being \mathcal{L} the supra-Laplace matrix. Through simple algebraic calculations, it is easy to show that such system has an equilibrium point at the origin, i.e., for $x_j = y_j = 0$ for every oscillator j .

Let us now restrict to the case $m = 1$, so that the nonlinear coupling term results in reality a linear one; let us observe that if $m > 1$, the linearization of the coupling term near the origin will vanish. Hence, by linearizing Eq. (B3) about $x_j = y_j = 0$ leads to

$$\frac{d}{dt} \begin{pmatrix} x_j \\ y_j \end{pmatrix} = \begin{pmatrix} \sigma_{\text{Re}} & -\sigma_{\text{Im}} \\ \sigma_{\text{Im}} & \sigma_{\text{Re}} \end{pmatrix} \begin{pmatrix} x_j \\ y_j \end{pmatrix} - \sum_{\ell} \mathcal{L}_{\ell j} \begin{pmatrix} \mu_{\text{Re}} & -\mu_{\text{Im}} \\ \mu_{\text{Im}} & \mu_{\text{Re}} \end{pmatrix} \begin{pmatrix} x_{\ell} \\ y_{\ell} \end{pmatrix}. \quad (\text{B4})$$

Disregarding the coupling term, the characteristic polynomial of the local system is

$$p(\lambda) = (\sigma_{\text{Re}} - \lambda)^2 + \sigma_{\text{Im}}^2, \quad (\text{B5})$$

with eigenvalues

$$\lambda = \sigma_{\text{Re}} \pm i\sigma_{\text{Im}}. \quad (\text{B6})$$

Hence, for $\sigma_{\text{Re}} < 0$, the origin is a stable solution.

Let now consider $\{\vec{\phi}^{(\alpha)}\}$ to be an orthonormal eigenbasis of $\bar{\mathbf{L}}$, i.e., $\bar{\mathbf{L}}\vec{\phi}^{(\alpha)} = \Lambda^{(\alpha)}\vec{\phi}^{(\alpha)}$, for $\alpha = 1, \dots, n$. Projecting the linear system onto the eigenbasis yields

$$\begin{cases} \frac{dx_j}{dt} = \sum_{\alpha} \frac{d\hat{x}_{\alpha}}{dt} \vec{\phi}_j^{(\alpha)} = \sum_{\alpha} (\sigma_{\text{Re}}\hat{x}_{\alpha} - \sigma_{\text{Im}}\hat{y}_{\alpha})\phi_j^{(\alpha)} - \sum_{\ell, \alpha} (\mu_{\text{Re}}\hat{x}_{\alpha} - \mu_{\text{Im}}\hat{y}_{\alpha})L_{j\alpha}\phi_{\ell}^{(\alpha)} \\ \frac{dy_j}{dt} = \sum_{\alpha} \frac{d\hat{y}_{\alpha}}{dt} \vec{\phi}_j^{(\alpha)} = \sum_{\alpha} (\sigma_{\text{Im}}\hat{x}_{\alpha} + \sigma_{\text{Re}}\hat{y}_{\alpha})\phi_j^{(\alpha)} - \sum_{\ell, \alpha} (\mu_{\text{Im}}\hat{x}_{\alpha} + \mu_{\text{Re}}\hat{y}_{\alpha})L_{j\alpha}\phi_{\ell}^{(\alpha)} \\ = \sum_{\alpha} (\sigma_{\text{Im}}\hat{x}_{\alpha} + \sigma_{\text{Re}}\hat{y}_{\alpha})\phi_j^{(\alpha)} - \sum_{\alpha} (\mu_{\text{Im}}\hat{x}_{\alpha} + \mu_{\text{Re}}\hat{y}_{\alpha})\Lambda^{(\alpha)}\phi_j^{(\alpha)}. \end{cases} \quad (\text{B7})$$

Then, exploiting the orthogonality of the eigenbasis, we obtain

$$\begin{cases} \frac{d\hat{x}_{\alpha}}{dt} = \sigma_{\text{Re}}\hat{x}_{\alpha} - \sigma_{\text{Im}}\hat{y}_{\alpha} - \Lambda^{(\alpha)}(\mu_{\text{Re}}\hat{x}_{\alpha} - \mu_{\text{Im}}\hat{y}_{\alpha}), \\ \frac{d\hat{y}_{\alpha}}{dt} = \sigma_{\text{Im}}\hat{x}_{\alpha} + \sigma_{\text{Re}}\hat{y}_{\alpha} - \Lambda^{(\alpha)}(\mu_{\text{Im}}\hat{x}_{\alpha} + \mu_{\text{Re}}\hat{y}_{\alpha}), \end{cases} \quad (\text{B8})$$

i.e., in a more compact form,

$$\frac{d}{dt} \begin{pmatrix} \hat{x}_{\alpha} \\ \hat{y}_{\alpha} \end{pmatrix} = \left[\begin{pmatrix} \sigma_{\text{Re}} & -\sigma_{\text{Im}} \\ \sigma_{\text{Im}} & \sigma_{\text{Re}} \end{pmatrix} - \Lambda^{(\alpha)} \begin{pmatrix} \mu_{\text{Re}} & -\mu_{\text{Im}} \\ \mu_{\text{Im}} & \mu_{\text{Re}} \end{pmatrix} \right] \begin{pmatrix} \hat{x}_{\alpha} \\ \hat{y}_{\alpha} \end{pmatrix} =: \mathbf{M}(\Lambda^{(\alpha)}) \begin{pmatrix} \hat{x}_{\alpha} \\ \hat{y}_{\alpha} \end{pmatrix}. \quad (\text{B9})$$

The eigenvalues of $\mathbf{M}(\Lambda^{(\alpha)})$, for each mode α , read

$$\lambda_{\alpha} = (\sigma_{\text{Re}} - \Lambda^{(\alpha)}\mu_{\text{Re}}) \pm i|\sigma_{\text{Im}} + \Lambda^{(\alpha)}\mu_{\text{Im}}|. \quad (\text{B10})$$

It follows that the homogeneous mode ($\Lambda^{(1)} = 0$) is stable for $\sigma_{\text{Re}} < 0$, while, since $\Lambda^{(\alpha)} > 0$, higher order modes ($\alpha > 1$) may become unstable if μ_{Re} is *sufficiently* positive, i.e., if

$$\mu_{\text{Re}} > -\frac{\sigma_{\text{Re}}}{\Lambda^{(\alpha)}}. \quad (\text{B11})$$

Equivalently, one may conclude that, once the dynamical parameters μ_{Re} and σ_{Re} are fixed, the condition for having instability reduces to requiring that the spectrum is sufficiently positive.

Finally, let us now show that the limit cycle does not exist if $\sigma_{\text{Re}} < 0$. Notice that, given $r_j^2 = x_j^2 + y_j^2$, we have

$$\begin{aligned} 2r_j\dot{r}_j &= 2x_j(\sigma_{\text{Re}}x_j - \sigma_{\text{Im}}y_j) - 2x_jr_j^2(\beta_{\text{Re}}x_j - \beta_{\text{Im}}y_j) + 2y_j(\sigma_{\text{Im}}x_j + \sigma_{\text{Re}}y_j) - 2y_jr_j^2(\beta_{\text{Im}}x_j + \beta_{\text{Re}}y_j) \\ &= 2x_j^2\sigma_{\text{Re}} - 2x_jy_j\sigma_{\text{Im}} - 2x_j^2r_j^2\beta_{\text{Re}} - 2x_jy_jr_j^2\beta_{\text{Im}} + 2x_jy_j\sigma_{\text{Im}} + 2y_j^2\sigma_{\text{Re}} - 2x_jy_jr_j^2\beta_{\text{Im}} - 2y_j^2r_j^2\beta_{\text{Re}} \\ &= 2r_j^2\sigma_{\text{Re}} - 2r_j^4\beta_{\text{Re}} = 2r_j^2(\sigma_{\text{Re}} - r_j^2\beta_{\text{Re}}), \end{aligned} \quad (\text{B12})$$

i.e.,

$$\dot{r}_j = r_j(\sigma_{\text{Re}} - r_j^2\beta_{\text{Re}}) =: f(r_j), \quad (\text{B13})$$

which is zero if either $r_j = 0$ or $r_j^2 = \frac{\sigma_{\text{Re}}}{\beta_{\text{Re}}}$. Notice that the first solution $r_j = 0$ is stable when $\sigma_{\text{Re}} < 0$. On the other hand, since $\sigma_{\text{Re}} < 0$, evaluating

$$f'(r_j) = \sigma_{\text{Re}} - 3r_j^2\beta_{\text{Re}}, \quad (\text{B14})$$

on the cycle radius $r_j^2 = \frac{\sigma_{\text{Re}}}{\beta_{\text{Re}}}$, leads to

$$f' \left(\sqrt{\frac{\sigma_{\text{Re}}}{\beta_{\text{Re}}}} \right) = -2\sigma_{\text{Re}} > 0. \quad (\text{B15})$$

Thus, for $\sigma_{\text{Re}} < 0$, the nontrivial limit cycle turns out to be unstable, and no stable oscillations exist near the origin. Consequently, any instability observed in the network is purely network-driven, not due to the intrinsic limit cycle of the individual oscillators.

Appendix C: Linear stability analysis of the Lorenz MWN

In this section, we provide the various conditions under which Turing patterns may emerge in the case of Lorenz oscillators coupled via MWNs. To achieve this goal we separately consider the six cases where $E_{ij} = 1$, for a given couple $i, j \in \{1, 2, 3\}$, $i \neq j$ and all the remaining entries vanish. For each case we determine the coefficients of the characteristic polynomial of the matrix $\mathbf{M}(\Lambda^{(\alpha)})$ and deduce the conditions for the Turing instability by using the Routh-Hurwitz criterion. To lighten the notation we will use in the following the variable $\gamma = \varepsilon \Lambda^{(\alpha)}$. Let us also recall that we assume

$$\sigma > \beta + 1 \text{ and } 1 < \rho < \rho_H = \frac{\sigma(\sigma + \beta + 3)}{\sigma - \beta - 1} \quad (\text{C1})$$

to ensure the stability of the equilibrium $\vec{x}^* = (\sqrt{\beta(\rho-1)}, \sqrt{\beta(\rho-1)}, \rho-1)^\top$.

1. Case $\mathbf{E}_{12} = 1$

From the definition of $\mathbf{M}(\gamma)$ given by (59) we get

$$\mathbf{M}(\gamma) = \begin{pmatrix} -\sigma & \sigma - \gamma & 0 \\ 1 & -1 & -x^* \\ y^* & x^* & -\beta \end{pmatrix}, \quad (\text{C2})$$

and thus the coefficients of the characteristic polynomial are given by

$$a_2 = \sigma + \beta + 1, \quad (\text{C3})$$

$$a_1 = \gamma + \beta\rho + \beta\sigma, \quad (\text{C4})$$

$$a_0 = \gamma\beta(2 - \rho) + 2\beta\sigma(\rho - 1). \quad (\text{C5})$$

We can observe that $a_2 > 0$ and $a_1 > 0$ are always positive. A necessary condition for the emergence of Turing patterns is thus $a_0 < 0$. By using the value of a_0 given by (C5) we can conclude that $a_0 < 0$ if

$$\varepsilon \Lambda^{(\alpha)} = \gamma > 2\sigma \frac{\rho - 1}{\rho - 2} = \gamma_{12}^{(\text{crit})} \text{ and } \rho > 2, \quad (\text{C6})$$

while if $\rho < 2$ then $a_0 > 0$ for all $\gamma > 0$, indeed (C5) returns

$$\frac{a_0}{\beta} = \gamma(2 - \rho) + 2\sigma(\rho - 1) > 0,$$

because we also have $\rho > 1$.

Let us now consider the last condition for the onset of Turing instability, $a_2 a_1 < a_0$. By using Eqs. (C3), (C4) and (C5) we obtain

$$\begin{aligned} a_2 a_1 - a_0 &= (\sigma + \beta + 1)(\gamma + \beta\rho + \beta\sigma) - \gamma\beta(2 - \rho) + 2\beta\sigma(\rho - 1) = \gamma[\sigma + \beta(\rho - 1) + 1] + \beta(\rho + \sigma)(\sigma + \beta + 1) - 2\sigma\beta(\rho - 1) = \\ &= \gamma[\sigma + \beta(\rho - 1) + 1] + \beta\rho(\beta + 1 - \sigma) + \sigma\beta(3 + \sigma + \beta) > 0. \end{aligned}$$

Hence $a_2 a_1 > a_0$. In conclusion Turing patterns can emerge if Eq. (C6) is satisfied.

2. Case $E_{13} = 1$

In this case, we get

$$\mathbf{M}(\gamma) = \begin{pmatrix} -\sigma & \sigma & -\gamma \\ 1 & -1 & -x^* \\ y^* & x^* & -\beta \end{pmatrix}, \quad (\text{C7})$$

and thus the coefficients of the characteristic polynomial are

$$\begin{aligned} a_2 &= \sigma + \beta + 1, \\ a_1 &= \beta\rho + \beta\sigma + \gamma\sqrt{\beta(\rho-1)}, \\ a_0 &= 2\gamma\sqrt{\beta(\rho-1)} + 2\beta\sigma(\rho-1). \end{aligned} \quad (\text{C8})$$

Because $\rho > 1$, we can thus straightforward realize that $a_2 > 0$, $a_1 > 0$ and $a_0 > 0$.

So Turing patterns emerge if and only if the last Routh-Hurwitz condition, $a_2a_1 - a_0 < 0$ is violated. A direct computation returns

$$a_2a_1 - a_0 = (\sigma + \beta + 1)[\beta(\rho + \sigma) + \gamma x^*] - [2\gamma x^* + 2\beta\sigma(\rho - 1)] = \beta[\rho(-\sigma + \beta + 1) + \sigma(\sigma + \beta + 3)] + \gamma x^*(\sigma + \beta - 1).$$

Let us remember that $\sigma > \beta + 1$ and thus $\sigma + \beta - 1 > 2\beta > 0$, moreover $\rho(\sigma - \beta - 1) < \sigma(\sigma + \beta + 3)$, we can thus conclude that

$$a_2a_1 - a_0 = \beta[\rho(-\sigma + \beta + 1) + \sigma(\sigma + \beta + 3)] + \gamma x^*(\sigma + \beta - 1) > 0.$$

In conclusion, in the case $E_{13} = 1$, Turing patterns never emerge.

3. Case $E_{21} = 1$

The matrix $\mathbf{M}(\gamma)$ is now given by

$$\mathbf{M}(\gamma) = \begin{pmatrix} -\sigma & \sigma & 0 \\ 1 - \gamma & -1 & -x^* \\ y^* & x^* & -\beta \end{pmatrix}. \quad (\text{C9})$$

The coefficients of the characteristic polynomial are

$$a_2 = \sigma + \beta + 1, \quad (\text{C10})$$

$$a_1 = \beta(\rho + \sigma) + \gamma\sigma, \quad (\text{C11})$$

$$a_0 = \beta[2\rho\sigma + \gamma\sigma - 2\sigma]. \quad (\text{C12})$$

Clearly $a_2 > 0$ and $a_1 > 0$, moreover

$$a_0 = \beta[2\rho\sigma + \gamma\sigma - 2\sigma] = \beta[2\sigma(\rho - 1) + \gamma\sigma -] > 0,$$

because $\rho > 1$. It remains to check the last condition, i.e.,

$$\begin{aligned} a_2a_1 - a_0 &= \\ &= (\sigma + \beta + 1)[\beta(\rho + \sigma) + \gamma\sigma] - \beta[2\rho\sigma + \gamma\sigma - 2\sigma] = \beta[\sigma\rho + \sigma^2 + \beta\rho + \beta\sigma + \rho + \sigma] + \gamma\sigma(\sigma + \beta + 1) - \beta[2\sigma(\rho - 1) + \gamma\sigma] = \\ &= \beta[-\rho(\sigma - \beta - 1) + \sigma(\sigma + \beta + 3)] + \gamma\sigma(\sigma + 1), \end{aligned}$$

by recalling again $\rho(\sigma - \beta - 1) < \sigma(\sigma + \beta + 3)$, we can conclude that $a_2a_1 - a_0 > 0$, hence not Turing patterns can develop in this case.

4. Case $E_{23} = 1$

In this case, the matrix $\mathbf{M}(\gamma)$ is

$$\mathbf{M}(\gamma) = \begin{pmatrix} -\sigma & \sigma & 0 \\ 1 & -1 & -x^* - \gamma \\ y^* & x^* & -\beta \end{pmatrix}, \quad (\text{C13})$$

and the coefficients of the characteristic polynomial are

$$\begin{aligned} a_2 &= \sigma + \beta + 1, \\ a_1 &= \beta(\rho + \sigma) + \gamma\sqrt{\beta(\rho - 1)}, \\ a_0 &= 2\beta\sigma(\rho - 1) + 2\gamma\sigma\sqrt{\beta(\rho - 1)}. \end{aligned} \quad (\text{C14})$$

The three coefficients a_2 , a_1 and a_0 are strictly positive, and therefore the emergence of patterns depends solely on the fourth Routh-Hurwitz condition based on the sign of $a_2a_1 - a_0$.

We then have

$$\begin{aligned} a_2a_1 - a_0 &= \\ &= (\sigma + \beta + 1)[\beta(\rho + \sigma) + \gamma x^*] - 2\sigma[\beta(\rho - 1) + \gamma x^*] = \gamma x^*(-\sigma + \beta + 1) + \beta[(\rho + \sigma)(\sigma + \beta + 1) - 2\sigma(\rho - 1)] = \\ &= -\gamma x^*(\sigma - \beta - 1) + \beta[-\rho(\sigma - \beta - 1) + \sigma(\sigma + \beta + 3)], \end{aligned}$$

observe that $\sigma - \beta - 1 > 0$ and $-\rho(\sigma - \beta - 1) + \sigma(\sigma + \beta + 3) > 0$, hence $a_2a_1 - a_0 < 0$ if

$$\varepsilon\Lambda^{(\alpha)} = \gamma > \beta \frac{\sigma(\sigma + \beta + 3) - \rho(\sigma - \beta - 1)}{x^*(\sigma - \beta - 1)} = \gamma_{23}^{(\text{crit})}, \quad (\text{C15})$$

5. Case $E_{31} = 1$

This case has already been considered in the main text; the aim of this section is to prove the negativity of γ_2 defined in Eq. (68), which is hereby recalled for the sake of simplicity.

$$\gamma_2 = 2\sqrt{\beta(\rho - 1)} - \frac{\beta(\rho + \sigma)(\beta + \sigma + 1)}{\sigma\sqrt{\beta(\rho - 1)}}.$$

Let us rewrite γ_2 as follows

$$\begin{aligned} \gamma_2 &= \frac{\beta}{\sigma\sqrt{\beta(\rho - 1)}} [2\sigma(\rho - 1) - (\rho + \sigma)(\beta + \sigma + 1)] = \frac{\beta}{\sigma\sqrt{\beta(\rho - 1)}} [2\rho\sigma - 2\sigma - \sigma(\beta + \sigma + 1) - \rho(\beta + 1) - \rho\sigma] = \\ &= \frac{\beta}{\sigma\sqrt{\beta(\rho - 1)}} [\rho(\sigma - \beta - 1) - \sigma(\beta + \sigma + 3)]. \end{aligned}$$

Let us recall that by assumption

$$\rho < \frac{\sigma(\sigma + \beta + 3)}{\sigma - \beta - 1},$$

from which it follows that $\gamma_2 < 0$.

6. Case $E_{32} = 1$

In this case we have

$$\mathbf{M}(\gamma) = \begin{pmatrix} -\sigma & \sigma & 0 \\ 1 & -1 & -x^* \\ y^* & x^* - \gamma & -\beta \end{pmatrix}, \quad (\text{C16})$$

and the coefficients of the characteristic polynomial are given by

$$\begin{aligned} a_2 &= \sigma + \beta + 1, \\ a_1 &= \beta(\rho + \sigma) - \gamma\sqrt{\beta(\rho - 1)}, \\ a_0 &= 2\beta\sigma(\rho - 1) - \gamma\sigma\sqrt{\beta(\rho - 1)}. \end{aligned} \quad (\text{C17})$$

One can easily realize that $a_0 < 0$ if

$$\varepsilon\Lambda^{(\alpha)} = \gamma > 2\sqrt{\beta(\rho - 1)} = x^*, \quad (\text{C18})$$

and $a_1 < 0$ if

$$\varepsilon\Lambda^{(\alpha)} = \gamma > \frac{\beta(\rho + \sigma)}{\sqrt{\beta(\rho - 1)}} = \gamma_{32}^{(\text{crit})}. \quad (\text{C19})$$

Moreover we have $a_2a_1 - a_0 < 0$ if and only if

$$\varepsilon\Lambda^{(\alpha)} = \gamma > \frac{\beta(\rho + \sigma)(\sigma + \beta + 1) + 2\sigma\beta(\rho - 1)}{(\beta + 1)\sqrt{\beta(\rho - 1)}} = \tilde{\gamma}_{32}^{(\text{crit})}.$$

In conclusion Turing patterns emerge if

$$\varepsilon\Lambda^{(\alpha)} > \min \left\{ x^*, \gamma_{32}^{(\text{crit})}, \tilde{\gamma}_{32}^{(\text{crit})} \right\}. \quad (\text{C20})$$